

Violations of the Weak Energy Condition for Lentz Warp Drives

Bill Celmaster
email: *bill.celmaster@verizon.net*

Steve Rubin
email: *slr42349@gmail.com*

(November 25, 2025)

Abstract

Warp drive spacetimes capable of superluminal transportation, were first introduced in 1994 by Miguel Alcubierre and then generalized by others. These spacetimes violated the Weak Energy Condition (WEC). Lentz proposed a new type of warp drive in 2020. It was claimed that this warp spacetime has non-negative energy density and can therefore be sourced by a classical plasma. We demonstrate that Lentz’s claim is incorrect. We begin with a direct calculation of the energy-momentum tensor of Lentz’s warp drive in a Eulerian reference frame, and show that there are spacetime regions where the energy density is negative. We then examine the theoretical basis of Lentz’s investigation and identify several derivation errors. The derivation errors can be somewhat ameliorated with a modified version of Lentz’s geometry, which more closely respects the equalities and inequalities discussed by Lentz. Even so, we show that the modified geometry still violates the WEC even in the Eulerian reference frame. We conclude with a brief discussion of no-go theorems and their relationship to geometries of the kind proposed by Lentz.

1 Introduction

In 1994, Miguel Alcubierre [1] described a kind of spacetime that contained a region he called a “warp drive”. Warp drives have several fascinating

properties. For example, an observer whose time line coincides with the center of the warp drive may have the same clock reading as observers outside the warp drive, that is, no time dilation, but is traveling at superluminal speed relative to those observers. Alcubierre then proceeded to show that these warp drive spacetimes have energy-momentum tensors that violate the weak energy condition¹ (WEC),

$$T_{\mu\nu}t^\mu t^\nu \geq 0, \tag{1}$$

where T is the energy-momentum tensor, and t is any timelike vector. It is generally believed that all classical physics theories have energy-momentum tensors satisfying the WEC and, in particular, that this holds for any classical plasma. If so, then the Alcubierre warp drive is either impossible or a consequence of some non-classical (exotic) theory. Quantum field theories are known to violate the WEC, but to date, no quantum warp drives have been described (see Barcelo et al. [2] and references therein).

Subsequent to the original Alcubierre paper, considerable research has explored alternate warp drives [3–16] and there is even work done towards the engineering of warp drives [17, 18]. Over time, various theorems have been proven showing that for very general classes of warp drive, the Weak Energy Condition (WEC) must be violated [6, 19, 20]. Moreover, superluminal motion is often associated with time travel (i.e., closed timelike curves). Although a variety of proposals – for general geometries – have been made for ways in which time travel could possibly avoid paradoxes (see, for example, the review by Shoshany [21]), it is commonly believed that physical theories should prohibit time travel. This principle has been named by Hawking [22] as “the chronology protection conjecture”. If a superluminal-capable warp drive were found to comply with the WEC, then we would still want to know whether it violates the chronology protection conjecture. The question of warp drives and time-travel has been the subject of considerable research [23–30]. For a large category of warp drives including those to be described in what follows, Shoshany [30] has proven that superluminal travel would indeed permit time travel under certain well-defined circumstances.

In 2020, Erik Lentz [31, 32] proposed a category of warp drives whose geometries are given in the ADM [33] formalism by specifying shift-vectors (as defined in, for example, Gourgoulhon [34]) obtained as gradients of potentials satisfying a certain hyperbolic differential equation but with various source

¹Alcubierre notes that other energy conditions are also violated but in this note, we limit discussion to the weak energy condition.

functions. Lentz then developed a number of relationships that he claimed are satisfied by all such warp drives, and from those relationships, he found a non-negativity condition that, if satisfied, would lead to a non-negative energy density as measured by an Eulerian observer. Finally, Lentz proposed a specific source function intended to satisfy the non-negativity condition, which should therefore lead to a warp drive geometry that Lentz claimed to satisfy the WEC. Lentz’s paper did not address the issue of time travel, but Shoshany [30] has proven that if Lentz’s warp drive could be built, then it could be configured for time travel.

Lentz’s interesting work has received a considerable amount of attention in the refereed physics literature [3, 5, 8–10, 12, 30, 35–39] as well as in the popular press [40–47]. Nevertheless, there is a disturbing question of why Lentz’s warp drive appears to violate the previously-mentioned WEC-violation theorem proven by Santiago et al. [20]. In fact, Santiago et al. proved an even stronger statement – namely, that a general class of warp drives with zero vorticity has a sometimes-negative Eulerian energy density. This appears to be in direct conflict with the claim made by Lentz, that his warp drive (which has zero vorticity) has a non-negative Eulerian energy density. Up to this point in time, the situation has remained confusing. Either the WEC-violation theorem is wrong, or Lentz’s warp drive doesn’t satisfy the conditions required for the WEC-violation theorem, or Lentz’s conclusions are wrong. In what follows, we resolve the matter by demonstrating that Lentz’s conclusions are wrong.

We will show by direct analysis of its energy-momentum tensor (as computed from the soliton geometry, via Einstein’s field equation) that the Lentz warp drive violates the WEC and, in particular, has regions of negative Eulerian energy density. Because these conclusions differ dramatically from those presented by Lentz [31], we present the analysis in detail. There are two key aspects of our demonstration. First, we show by numerical computation that the Lentz geometry violates the weak-energy condition. Second, we examine the various relationships that led to the conclusion in Ref. [31], that the energy density is non-negative. It turns out that several of those relationships are incorrect.

In Section 2, we introduce a class of warp drives described by Natário, [6] which generalizes Alcubierre’s [1] original warp drive, and we provide some of the key geometric quantities to be used in the subsequent analysis. In Section 3, we review the defining characteristics – such as the differential equation to be solved by the potential whose gradient is the shift vector

– of Lentz’s warp drive geometries. We then examine Lentz’s rhomboidal source (LRS) warp drive and show that its Eulerian energy has regions of negativity, thus violating the WEC. We point out that this might be due to the fact that the LRS geometry does not in fact satisfy Lentz’s warp-drive defining characteristics. In Section 4, we introduce a class of geometries that (mostly) satisfy Lentz’s warp-drive defining characteristics. We then turn to the question of why Lentz expected his warp drive to satisfy the WEC. In Ref. [31], Lentz derived a number of equations and inequalities that lead to criteria for WEC-compliance. However, the LRS warp drive does not satisfy these criteria. In Section 4 we show that Lentz made several mistakes in the derivations of the expressions that led him to his WEC-compliance criteria. In Section 5 we introduce and examine a modified version (MLRS) of the LRS warp drive. This modified version is a member of the class of geometries considered in the previous section, also based on a rhomboidal source such as Lentz’s original proposal. We show that this warp drive violates the equations, inequalities and properties proposed by Lentz, and that in the previous section were seen to be generally incorrect. In Section 6 we replace the rhomboids by rectangles to determine whether our conclusions are sensitive to the type of source function chosen. Again, this geometry violates the WEC, but the non-zero regions of energy density are highly concentrated near the vertex points. This example is noteworthy because it significantly differs from the energy distribution of Alcubierre’s ([1]) original warp drive. The last topic we explore, in Section 7, is the question of whether no-go theorems should apply to the warp drives considered in this paper. If so, do those no-go theorems depend on the conditions that, if relaxed, could violate those theorems and therefore allow a WEC-compliant warp drive? Here, we briefly address these possibilities.

2 Natário warp drives and the Eulerian energy density condition

We limit our discussion to the spacetimes described by Natário, [6] which dominate most of the literature on warp drives. These spacetimes have line elements,

$$ds^2 = -(1 - N^i N_i) dt^2 - 2N_i dx^i dt + \sum_{i=1}^3 dx^{i2}, \quad (2)$$

where we have written the line element using the convention of the ADM formalism [33], where the shift vector N_i is a function of space and time.² Spacetime is foliated into flat spacelike hypersurfaces of constant t . Coordinates on the hypersurfaces are indexed using Latin letters and, because the hypersurfaces are flat, all hypersurface raising and lowering operators are identity operators. So, for example, $N_i = N^i$. For certain values of the shift vectors, the resulting spacetimes describe warp drives of the type introduced by Alcubierre [1]. We now define some tensors that are important in the analysis.

The normal vector n is defined as

$$n^\mu = (1, N^i), \quad (3)$$

where we adopt the convention that Greek indices refer to space-time and as mentioned above, Latin indices refer to the spatial coordinates of the level- t hypersurfaces. Note that the normal vector is timelike. If the observers have a 4-velocity n^μ , we refer to them as *Eulerian observers*.

We also introduce the extrinsic curvature tensor for a particular hypersurface $t = \text{constant}$. It is defined as

$$K_{ij} = \frac{1}{2} (\partial_i N_j + \partial_j N_i). \quad (4)$$

Recall from Eq. (1) that the weak energy condition requires $T_{\mu\nu} t^\mu t^\nu \geq 0$ for all time-like vectors t . A fortiori, $T_{\mu\nu} n^\mu n^\nu \geq 0$. This quantity, $T_{\mu\nu} n^\mu n^\nu$ is known as the Eulerian energy density E (i.e. the energy density as measured by a Eulerian observer), and the inequality $T_{\mu\nu} n^\mu n^\nu \geq 0$ is “the Eulerian energy density condition”.

Clearly, to prove that the WEC inequality is obeyed, we must demonstrate the inequality for **all** timelike vectors, and it is insufficient to establish the inequality only for the Eulerian energy density. However, to prove that the WEC is violated, it suffices to demonstrate the violation of the Eulerian energy density condition. This is what we will show in the sections which follow.³

²The sign of the shift-vector is a matter of convention. We have adopted the convention used by Lentz. This choice has no impact on the sign of the Eulerian energy density.

³Note that Lentz [31] claims to show that his warp drive has a non-negative Eulerian energy density. Had his conclusion been correct, it still wouldn't have established the validity of the WEC, since other time-like vectors would have needed to be considered.

One of the virtues of the ADM formalism is that it permits Einstein's equations to be formulated purely in terms of the extrinsic tensor. It can be shown (for example, seeourgoulhon [34]) that

$$8\pi E = \frac{1}{2} (-K_i^j K_j^i + K^2), \quad (5)$$

where E is the Eulerian energy density.

3 Lentz's original warp drive

In his paper [31], Lentz proposed a warp-drive geometry that he argued had a non-negative energy density. His non-negativity argument depends on constructing the geometry from a potential function ϕ that meets several criteria, including being a solution to a differential equation – Eq. (6) below – with a rhomboidal source function ρ_{rhomb} – Eq. (8) below. Lentz then presents a potential function ϕ_L that he claims satisfies the solution criteria. He next claims to show, by numerical computation and display of the Eulerian energy density, that his geometry satisfies the WEC. We demonstrated that Lentz made a mistake in his computation of the energy density, and that in fact, it is not positive and violates the WEC. Lentz's mistake arises, in part, from the fact that ϕ_L is **not** a solution to Eq. (6), and not even approximately. Because Lentz's WEC compliance (non-negativity) argument was supposedly derived from the solutions of Eq. (6), it is not surprising that an incorrect solution to that equation leads to a WEC violation.

In Section 5, we propose a modified version of ϕ_L that closely resembles what Lentz presumably had in mind. The function ϕ_{rh} is a solution to Eq. (6) almost everywhere (however, we were unable to find a solution for all values of the coordinates).

3.1 The warp drive hyperbolic differential equation

Lentz [31] defined a potential function $\tilde{\phi}$ as a solution to the hyperbolic differential equation (Eq.(15) in Ref. [31])

$$\partial_x^2 \tilde{\phi} + \partial_y^2 \tilde{\phi} - \frac{2}{v_h^2} \partial_z^2 \tilde{\phi} = \tilde{\rho}, \quad (6)$$

where $\tilde{\rho}$ denotes the specified source function. For later reference, we refer to Eq. (6) as “Lentz’s differential equation”. The warp geometry is obtained by substituting the shift vector

$$\mathbf{N} = \nabla\tilde{\phi} \tag{7}$$

into the metric defined in Eq. (2). Lentz then imposes additional conditions on $\tilde{\phi}$ for which it is a unique solution. One of these conditions is on the boundary $\tilde{\phi} \rightarrow 0$ as $z \rightarrow -\infty$. The second condition is a constraint that reduces the dimensionality of the function domains; namely, $\tilde{\rho}$ can be written as⁴ $\tilde{\rho}(x, y, z) = \rho(s(x, y), z) = \rho(-s(x, y), z)$ and $\tilde{\phi}$ can be written as $\tilde{\phi}(x, y, z) = \hat{\phi}(s(x, y), z)$, where $s(x, y) = |x| + |y|$, which implies that the solution $\tilde{\phi}$ should be symmetric under the exchange of x and y . Finally, Lentz makes $\tilde{\rho}$ and $\tilde{\phi}$ implicit functions of time, by setting $(x, y, z) \rightarrow (x, y, z - vt)$. We refer to $\mathbf{v} = (0, 0, v)$ as the “velocity of the warp drive.”

3.2 Lentz’s rhomboidal source

The remaining step in specifying the Lentz metric is to select the source. At this stage, we must point out that Lentz does not provide an analytical definition of his source. Therefore, we constructed a source ρ_{rhomb} , that resembles Lentz’ as closely as possible based on the information provided. Lentz chooses his source as a function of $|x| + |y|$ and z . He also describes it as consisting of rhomboids in the $y = 0$ plane, and then provides a picture, Fig. (1) in ref. [31]. One of our challenges was to find an analytical form for ρ_{rhomb} which results in a picture similar to that of Lentz.⁵

The source function must also be such that the resultant shift vector \mathbf{N} has the following properties.

1. The z -component N_z of the shift vector is non-zero and level over a finite region about the origin (which Lentz refers to as the “central region”),

⁴Although Lentz doesn’t explicitly state the condition $\rho(s(x, y), z) = \rho(-s(x, y), z)$, it can be inferred from his Fig. (1).

⁵To further verify that we have used a source virtually identical to Lentz’s we note below that the x and z components of the shift vector resemble their counterparts plotted in ref. [31]. The sign difference turns out to be due the fact that Lentz’s figure of N_x is inconsistent with his Eq. (20), in that the signs are reversed.

2. The x and y -components of the shift vector are zero over the same region.

A further requirement is that Eulerian observers in the central region move synchronously with the warp drive. This requirement is satisfied by including in the definition of ρ_{rhomb} an overall scale factor $W = v/N_z(0,0,0)$, where v is the z -component of the warp drive velocity (as described in Section 3.1). We note that this is only approximately true for the rhomboidal source described below, because properties 1 and 2 above are only approximately true. However, in Section 6, we provide an alternative source such that these conditions hold exactly over a broader region. In the body of this paper, we will not further discuss time-dependence or velocity, but in Appendix H we show how the class of observers just described, experience travel, including superluminal travel, without time dilation.

Here is the analytic form that we used for the rhomboidal-source function.

$$\rho_{\text{rhomb}}(s, z) = \tilde{\rho}_{\text{rhomb}}(x, y, z) = W \sum_{i=1}^4 \alpha_i \Theta(p_i(s, z)) g_i(s), \quad (8)$$

where Θ is the Heaviside function and

$$p_i(s, z) = L_x - \frac{L_x}{L_z} |z - \xi_i| - ||s| - \beta_i|, \quad (9)$$

and

$$g_i(s) = Q_{\min} + (Q_{\max} - Q_{\min}) (|s| - \beta_i)^2, \quad (10)$$

where:

- W is the overall scale factor, described above.
- $s = |x| + |y|$
- L_x is the semi-length of the rhomboids along the x -direction.
- L_z is the semi-length of the rhomboids along the z -direction.
- α_i are weights that may be negative or positive
- β_i are the s -coordinates of the rhomboid centroids.
- ξ_i are the z -coordinates of the rhomboid centroids.

- Q_{\max} and Q_{\min} are the maximum and minimum charge, respectively.

In addition, this source configuration satisfies the following constraints:

- Rhomboids are elongated along the x -direction and narrow along the z -direction, as shown in Fig. (1) in ref. [31], i.e. $L_x \gg L_z$.
- Rhomboids are equally spaced along the z -direction, that is $\Delta\xi$ is a constant, where $\Delta\xi$ is the difference in ξ_i between any rhomboid and its nearest neighbor along the z -direction. For any such pair of rhomboids, the corresponding difference $\Delta\beta$ is also constant. This implies that the line joining the centroids of any such pair of rhomboids creates a constant angle $\theta = \arctan(\pm\Delta\beta/\Delta\xi)$ with the z -axis.

Note: It will be seen that, in order to guarantee that the potential ϕ and the shift vector N_i are bounded (at $y = 0$ in Lentz's original ansatz and for all y in the corrected ansatz presented in Section 4), it is necessary that $\theta = \arctan(\pm 1/v_h)$. Therefore, as a consequence of setting $v_h = 1$, we must have $\theta = \pm 45^\circ$ or equivalently, $\Delta\beta = \pm\Delta\xi$. The choices for the rhomboid centroids (β_i, ξ_i) , shown in the table below, reflect this more stringent constraint.

- Rhomboids do not overlap, i.e. $\Delta\xi \geq L_z$ and, unless $\beta_i = 0$, $|\beta_i| \geq L_x$
- The total integrated charge of the system is zero, implying that $\sum_{i=1}^4 \alpha_i = 0$, where $\alpha_i \neq 0$ for all i .

The source configuration is such that a rotation of 180° about the z -axis leaves the rhomboids unchanged, that is unless $\beta_i = 0$, the β_i come in pairs such that, for each rhomboid with parameters β_i, α_i, ξ_i , there is another rhomboid with parameters $-\beta_i, \alpha_i, \xi_i$. Thus, as a result of the preceding constraints, Eqs. (9) and (10) imply that the complete source configuration comprises seven rhomboids.

For the computational results that follow (see Appendices C, D, G), we used the following values for the parameters, which satisfy the definitions and constraints discussed above.

Parameter	Value(s)			
i	1	2	3	4
β_i	1	2	1	0
ξ_i	-1	0	1	2
α_i	25	-25	-25	50
L_x	1			
L_z	1/8			
W	$v/N_z(0, 0, 0)$, $v = 1$			
Q_{\max}, Q_{\min}	1, 1/4			

The rhomboid source, as described in Eqs. (8), (9) and (10), is displayed in Fig.(1), except that it was not scaled by W . That is, the figure shows $\tilde{\rho}_{\text{rhomb}}/W$, which is equivalent to $\tilde{\rho}_{\text{rhomb}}N_z(0, 0, 0)$, as $v = 1$. We do this so that the figure may be more easily compared to Lentz's Fig. 1.

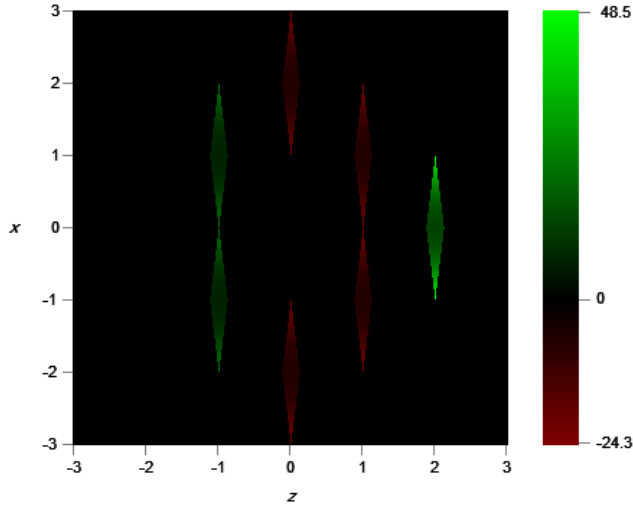


Figure 1: Unscaled rhomboidal source $\tilde{\rho}_{\text{rhomb}}N_z(0, 0, 0)$ for $y = 0$

As mentioned earlier, when we compare Fig. (1) to Fig. (1) in ref. [31], we can see that the two source functions appear very close to one another. We also varied some of the parameters of ρ_{rhomb} to see how these parameters would affect our conclusions, and found no qualitative differences.

3.3 Lentz's potential, ϕ_L

In this section, we begin with Lentz's function ϕ_L and carefully use it to build a warp geometry. Subsequently, we compute the Eulerian energy density. Despite using the same geometry as Lentz, we do not obtain the non-negative result that he shows in [31]. We trace this discrepancy in part to a sign error (see Appendix A) that Lentz made in one of the terms that he uses in his calculation, which is ultimately caused by the fact that ϕ_L is not a solution of Lentz's differential equation, Eq. (6). Moreover, had Lentz displayed his result at greater γ -correction (see Appendix G), his 'positive' result (using the wrong sign) would have revealed some regions of negativity.

Lentz [31] defines the potential $\phi_L(x, y, z)$ by setting

$$\phi_L(x, y, z(t)) = \frac{1}{4v_h} \int_{-\infty}^{\infty} dx' dz' \Theta \left(z(t) - z' - \frac{1}{v_h} |x - x'| \right) \rho_{\text{rhomb}}(|x'| + |y|, z'(t)), \quad (11)$$

where $z(t) = z - vt$ and v is the speed of the warp drive. This is equivalent to Eq. (18) in ref. [31]. In this section, we set $v_h = 1$. Lentz claimed that ϕ_L is a solution to the differential equation in Eq. (6) with the source in Eq. (8) and under the conditions specified in Subsection (2). As shown in Appendix A, this claim is false. **ϕ_L is not a solution.** As an example of one of the ways in which the claim is false, note that ϕ_L is not symmetric under the exchange of x and y , and therefore violates one of Lentz's solution conditions.

We computed the Eulerian energy, by first computing the shift vector. We substitute ρ_{rhomb} into the expression for ϕ_L given by Eq. (11) and then computing the shift vector by applying Eq. (7). Details of the calculations are provided in Appendix C.

The rhomboidal-source shift-vector component N_z^L is displayed in Fig.(2).

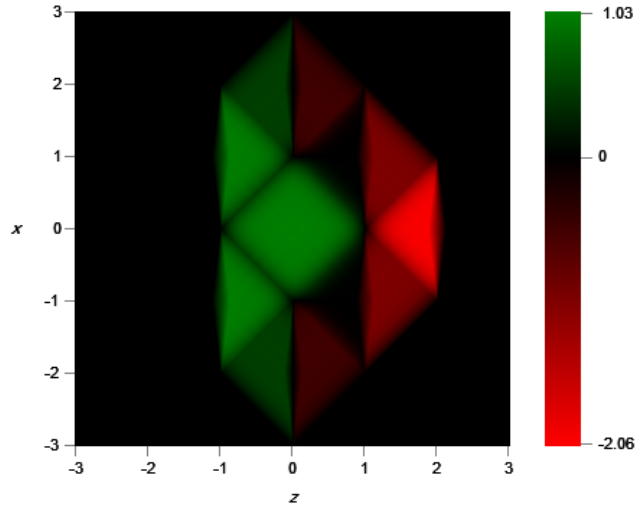


Figure 2: N_z^L for the rhomboidal source, evaluated on the slice $y=0$.

This figure can be compared with the left-hand side of Fig. (2) in Lentz [31]:⁶ We see that the plots are very similar. We also compared N_x^L with Lentz's figure for N_x^L (right-hand side of Fig. (2) of Lentz [31]). The results are shown in Fig. (3).

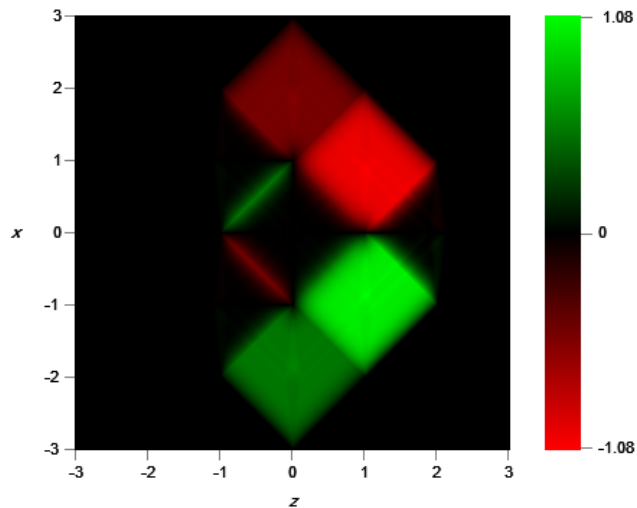


Figure 3: N_x^L for the rhomboidal source, evaluated on the slice $y = 0$.

⁶Our definition of \mathbf{N} already includes the factor $v/N_z(0,0,0)$ that Lentz shows explicitly, where $v = 1$. (This note also applies to Fig. (3).)

It turns out that Lentz’s figure of N_x^L is inconsistent with his Eq. (20), in that the signs are reversed. Nevertheless, it is structurally the same as our result and thus provides further evidence that our source function must be close to that of Lentz.⁷

Finally, we computed the Eulerian energy density E_L using Eqs. (5) and (4) respectively. This computation was performed using the analytical methods described in Appendix C for the first derivatives and in Appendix D for the second derivatives. Note that E_L is ambiguous (not uniquely defined) for certain sets of points including the plane $y = 0$, owing to discontinuities in N_y (See Appendix I). We address the issue of discontinuities more fully in the next section and Appendix D. In addition, as shown in Fig. (4), we avoided the ambiguity on the $y = 0$ plane by displaying E_L for $y = 1.0 \times 10^{-6}$.

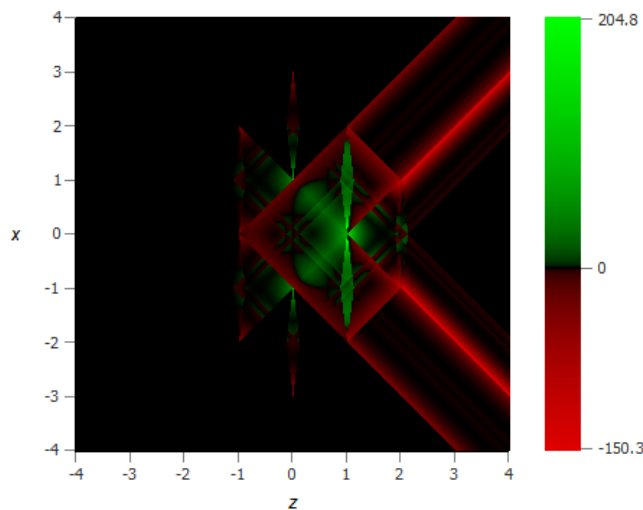


Figure 4: Rhomboidal-source Eulerian energy density at $y = 1.0 \times 10^{-6}$.
($\gamma = 0.43$)

It can be observed from Fig. (4) that there are regions of both positive and negative energy densities; therefore, this warp drive violates the WEC.

Note that in Fig. (3) of Lentz [31], the Eulerian energy density appears very different, and in fact looks non-negative. Since this figure is offered as one of the main conclusions of Lentz’s paper – namely, that the Lentz geometry

⁷As far as we can tell, none of Lentz’s other results are sensitive to this sign-inconsistency.

is WEC compliant – it is important to re-emphasize that Lentz’s figure is **not** correctly derived from his geometry, and to give a detailed explanation of why. We believe that there are two significant errors that contribute to Lentz’s incorrect demonstration of energy positivity.

- Lentz uses his Eq. (17) to obtain his Fig. (3), an assumption we have made based on the fact that we can reproduce the apparent positive energy density shown in his Fig. (3) using Eq. (17) to compute the Eulerian energy density, and then displaying the result by setting $\gamma = 1$ (no gamma correction). However, Lentz’s Eq. (17) is not the correct equation for the energy density of the geometry. The equation is derived by assuming that ϕ_L is a solution of Lentz’s differential equation – Eq. (6). As previously mentioned, this assumption is false. In particular, the illusion of a positive energy density is largely the result of an overall sign error in the expression for ϕ_L , as mentioned at the beginning of this section and demonstrated in Appendix A.
- Although Fig. (3) of Lentz [31] shows a positive energy density everywhere, this is an artifact of the graphical display, assuming that Lentz employed his Eq. (17), as previously discussed. When we display that result by setting γ to low values (greater correction), we can clearly see regions of negativity that are almost invisible for $\gamma = 1$.

There is one more observation regarding our display – Fig. (4) for Eulerian energy density. We can see that the energy density does not appear confined close to the region where the source is non-zero. In fact, there are two 45° bands extending to large positive values of z which presumably extend to infinity. (To make this more obvious, we show a broader region of space than in other figures.) Similar results were observed for the other values of y . Consequently, the energy obtained by integrating the energy density, is infinite. This fact violates an implicit, and hitherto unmentioned, requirement of the potential, namely, that it must result in a geometry with a finite total energy. Why does finite-energy violation occur? In Ref. [31], Lentz speaks of how “sources are organized to terminate the stray branches of the wave cone”. However, because of the asymmetry between x and y , this precise organization becomes increasingly distorted as y gets further away from zero. For further discussion on this asymmetry, see Appendix A.1.

4 Properties of hyperbolic potential (HP) warp drives

We turn now to Lentz’s non-negativity “derivations”⁸ for a class of warp geometries based on shift vectors $\mathbf{N} = \nabla\phi$ where

$$\phi(x, y, z) = -\frac{1}{4} \int_{-\infty}^{+\infty} \int_{-\infty}^{+\infty} ds' dz' \Theta(z - z' - |s(x, y) - s'|) \rho(s', z'), \quad (12)$$

and $s(x, y) = |x| + |y|$, $\rho(s(x, y), z) = \tilde{\rho}(x, y, z)$ and ρ is the source function to be specified. We refer to such potentials ϕ as “hyperbolic potentials” (HP). We will examine the properties of HP geometries, including the number of relationships from which Lentz incorrectly concluded that certain HP geometries must satisfy the WEC. We will see that these claims are incorrect.

4.1 HP warp drives almost satisfy the Lentz DE

By taking appropriate the derivatives of ϕ , we can show that it satisfies Lentz’s differential equation Eq. (6) almost everywhere.⁹ The following identities prove useful.¹⁰

$$\begin{aligned} \partial_x f(s(x, y), z) &= \partial_s f(s, z) \operatorname{sgn}(x), \\ \partial_y f(s(x, y), z) &= \partial_s f(s, z) \operatorname{sgn}(y), \\ \partial_s \phi &= \frac{1}{4} \int_{-\infty}^{\infty} ds' \operatorname{sgn}(s - s') \rho(s', z - |s - s'|), \end{aligned} \quad (13)$$

for any differentiable function f . After some manipulations (some of which are presented in Appendix A), we obtain

$$\partial_x^2 \phi + \partial_y^2 \phi - 2\partial_z^2 \phi = \rho(s, z) + S(x, y, z) \quad (14)$$

⁸We have put quotation marks around the word “derivations”, because – as we shall see – some of the “derivations” are incorrect.

⁹We use the (non-standard) phrase *almost everywhere* to mean “everywhere except for delta functions.”

¹⁰We have used the distribution equality $\partial_x |x| = \operatorname{sgn}(x)$. It is also common to write this equality as $\partial_x |x| = \frac{x}{|x|}$. Since these expressions are discontinuous at $x = 0$, there is an ambiguity (explained earlier in the text) about how to extend the expressions to $x = 0$. Considered as distributions, all finite definitions will be equivalent, so we won’t offer a definition for $x = 0$ other than to require finiteness.

where

$$S(x, y, z) = 2(\delta(x) + \delta(y)) \partial_s \phi = \frac{1}{2} (\delta(x) + \delta(y)) \int_{-\infty}^{+\infty} ds' \operatorname{sgn}(s-s') \rho(s', z-|s-s'|). \quad (15)$$

This demonstrates that ϕ is a solution to Lentz's differential equation, except when $x = 0$ or $y = 0$. These boundary terms are physically consequential. We were unable to find a closed-form potential $\tilde{\phi}$ that solved Lentz's differential equation.

4.2 Energy density of HP warp drives

In this section, we derive the following: if ϕ is a solution to Eq. (14), the energy density E is given by

$$E = \frac{1}{8\pi} [T(x, y, z) + U(x, y, z)] \quad (16)$$

where

$$T(x, y, z) = S(x, y, z) (\partial_s^2 \phi + \partial_z^2 \phi) + 4\delta(x)\delta(y) (\partial_s \phi)^2. \quad (17)$$

and

$$U(x, y, z) = (\rho(s, z) + 2\partial_z^2 \phi) \partial_z^2 \phi - 2(\partial_z \partial_s \phi)^2. \quad (18)$$

This expression for energy density contains the term U which is similar to Lentz's Eq. (17) but also adds the term $T(x, y, z)$, which is zero almost everywhere⁹ and is proportional to delta functions. As we will see later, the delta functions can contribute significantly to the total energy.

Our derivation of Eqs. (16) - (18), starts with the Eulerian energy density, E , as given by Eqs. (4) and (5) as follows:

$$8\pi E = \frac{1}{2} (-K_i^j K_j^i + K^2),$$

where

$$K_{ij} = \frac{1}{2} (\partial_i N_j + \partial_j N_i),$$

with the shift-vector given by Eq. (7)

$$\mathbf{N} = \nabla \phi.$$

Expanding all the terms, we get

$$E = \frac{1}{8\pi} (\partial_x^2 \phi \partial_y^2 \phi + (\partial_x^2 \phi + \partial_y^2 \phi) \partial_z^2 \phi - (\partial_x \partial_y \phi)^2 - (\partial_x \partial_z \phi)^2 - (\partial_z \partial_y \phi)^2). \quad (19)$$

Then we use Eq. (14) above to substitute for $(\partial_x^2 \phi + \partial_y^2 \phi)$.

$$E = \frac{1}{8\pi} (\partial_x^2 \phi \partial_y^2 \phi + (\rho(s, z) + 2\partial_z^2 \phi + S(x, y, z)) \partial_z^2 \phi - (\partial_x \partial_y \phi)^2 - (\partial_x \partial_z \phi)^2 - (\partial_z \partial_y \phi)^2). \quad (20)$$

To further modify the above expression for E , note that

$$\begin{aligned} \partial_x^2 \phi &= \partial_x (\text{sgn}(x) \partial_s \phi) = 2\delta(x) \partial_s \phi + \partial_s^2 \phi. \\ \partial_y^2 \phi &= 2\delta(y) \partial_s \phi + \partial_s^2 \phi. \\ \partial_x \partial_y \phi &= \text{sgn}(x) \text{sgn}(y) \partial_s^2 \phi. \\ \partial_z \partial_x \phi &= \text{sgn}(x) \partial_s \partial_z \phi. \\ \partial_z \partial_y \phi &= \text{sgn}(y) \partial_s \partial_z \phi. \end{aligned} \quad (21)$$

Substituting in Eq. (20), we obtain Eqs. (16), (17) and (18).

4.3 Finiteness of the energy of HP warp drives

One of the requirements for the stress tensor, and therefore for the potential ϕ above, is that the total energy is finite in any reference frame. This condition is satisfied provided that the source function ρ in Eq. (12) satisfies the following three conditions:

- The linear-cancellation condition

$$\int_{-\infty}^{\infty} ds' \rho(s', \alpha \pm s') = 0 \quad (22)$$

for any constant α .

- The source-domain boundedness condition

$$\begin{aligned} \rho \text{ has a bounded domain such that } \rho(s, z) &= 0 \\ \text{if } |z| > B \text{ or } |s| > B \end{aligned} \quad (23)$$

for some B .

- $s(x, y) = |x| + |y|$

In Appendix J, we demonstrate that, when these conditions hold, the shift vector components have a bounded domain. That is, there exists a bound C , such that $N_i(x, y, z) = 0$ unless $|x|, |y|, |z| \leq C$. From this, it follows that the stress tensor has a bounded domain and thus, the integral of $T^{\mu\nu}t_\mu t_\nu$ for timelike t , is finite over any spatial slice.

For Lentz's original warp drive, introduced in the previous section, the boundedness of the shift vector component N_z^L is portrayed at $y = 0$ in Fig.(2). Similarly, for N_x in Fig.(3). However, in Lentz's original warp drive, this boundedness is only true at $y = 0$. At the other values of y the shift vector is unbounded. We have observed this implicitly in Fig.(4), where the Lentz warp-drive energy density appears unbounded when $y = 1.0 \times 10^{-6}$.

4.4 The energy non-negativity condition and shift-derivative inequality

Lentz proposed the inequality, in his Eq. (13), which is a non-negativity condition for the Eulerian energy density. Lentz's inequality depends on a shift-derivative inequality $(\partial_z^2 \phi)^2 \geq (\partial_z \partial_s \phi)^2$, which is false in many cases including our rhomboidal geometry introduced in the next section. Moreover, even when this assumption is true, Lentz's theorem fails when $x = 0$ or $y = 0$. This failure has serious consequences for Lentz's non-negativity condition. The remainder of this section elaborates on this summary.

4.4.1 The shift-derivative inequality

The shift-derivative inequality is

$$(\partial_z^2 \phi)^2 \geq (\partial_z \partial_s \phi)^2. \quad (24)$$

Lentz [31] claims (see the text between his Eqs. (19) and (20)) that he has proven a version of this and that it can be derived from Eqs. (19) and (20) of his paper.

However, there is a flaw in Lentz's proof of his shift-derivative inequality, which is not generally true (neither is Eq. (24)). We now review Lentz's argument.

We begin with the shift-vector components. These are derived in Appendix B and are similar to those in Lentz's Eqs. (19) and (20) respectively.

$$\begin{aligned} N_x &= \partial_x \phi = \text{sgn}(x) \partial_s \phi = \frac{1}{4} \text{sgn}(x) \int ds' \text{sgn}(s - s') \rho(s', z - |s - s'|), \\ N_y &= \partial_y \phi = \text{sgn}(y) \partial_s \phi = \frac{1}{4} \text{sgn}(y) \int ds' \text{sgn}(s - s') \rho(s', z - |s - s'|), \\ N_z &= \partial_z \phi = -\frac{1}{4} \int ds' \rho(s', z - |s - s'|), \end{aligned} \quad (25)$$

If we take the z derivatives of both sides, and then the absolute values, we obtain

$$\begin{aligned} |\partial_z^2 \phi| &= \frac{1}{4} \left| \int ds' \partial_z \rho(s', z - |s - s'|) \right| \\ |\partial_z \partial_x \phi| &= \frac{1}{4} \left| \int ds' \text{sgn}(s - s') \partial_z \rho(s', z - |s - s'|) \right| \\ |\partial_z \partial_y \phi| &= |\partial_z \partial_x \phi| \end{aligned} \quad (26)$$

When comparing the first two equations above, we note that the integrands differ only by $\text{sgn}(s - s')$. Because $1 \geq \text{sgn}(s - s')$ it might be tempting to think that the first integral is greater than the second. However, such an inequality generally does not hold. We demonstrate this in Appendix F by providing a counterexample.

4.4.2 The energy non-negativity condition

A correct energy-density inequality can be stated as follows: if ϕ is a solution of Eq. (14) and if $(\partial_z^2 \phi)^2 \geq (\partial_z \partial_s \phi)^2$, then

$$E \geq \frac{1}{8\pi} (T(x, y, z) + \rho(s, z) \partial_z^2 \phi). \quad (27)$$

We refer to this as Lentz's "modified non-negativity inequality". This resembles Lentz's Eq.(21) (up to an overall factor of $\frac{1}{8\pi}$), except for the term $T(x, y, z)$ which is 0 almost everywhere.⁹ Eq. (27) can be derived as follows:

- From Eq. (4.2), $E = \frac{1}{8\pi} [T(x, y, z) + U(x, y, z)]$

- From Eq. (18),

$$U(x, y, z) = \rho(s, z) \partial_z^2 \phi + \alpha, \quad (28)$$

where $\alpha = 2 \left((\partial_z^2 \phi)^2 - (\partial_z \partial_s \phi)^2 \right)$

- Therefore $E = \frac{1}{8\pi} (T(x, y, z) + \rho(s, z)\partial_z^2\phi + \alpha)$
- According to Eq. (24), $\alpha \geq 0$, thus proving Eq. (27).

The inequality Eq. (27) yields a general non-negativity condition: If the RHS is non-negative, then the Eulerian energy density E will be non-negative, provided that ϕ is a solution of Lentz's differential equation and that the shift-derivative equality is obeyed. We see in Fig. (5), for ϕ_L , the RHS is positive. However, ϕ_L is **not** a solution of the Lentz differential equation. Among other problems, it has the wrong sign. Therefore, we can conclude nothing from Eq. (27), about the sign of the energy density for the ϕ_L geometry.

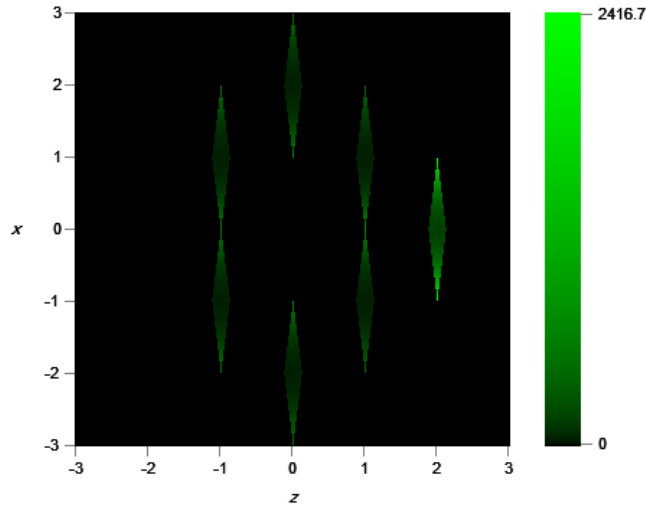


Figure 5: $\rho_L \partial_z^2 \phi_L$ for $y = 10^{-6}$ ($\gamma = 0.43$)

Lentz's original non-negativity equation¹¹ only contains the second term, $\frac{1}{8\pi}\rho(s, z)\partial_z^2\phi$ of the modified energy inequality. However, even if the term is positive, it could happen that the first term, $\frac{1}{8\pi}T(x, y, z)$ has regions of negativity. We show an example of this in the next section, where we consider a rhomboidal source.

¹¹See Eq. (21) of Lentz [31]

5 A modified version of Lentz's geometry

5.1 The modified potential, ϕ_{rh}

Consider the HP potential ϕ_{rh} obtained from Eq. (12) with the source function $\rho_{\text{rhomb}}(s, z(t))$ defined in Eqs. (8) – (10).

$$\phi_{\text{rh}}(x, y, z(t)) = -\frac{1}{4}v_h \int_{-\infty}^{+\infty} \int_{-\infty}^{+\infty} ds' dz' \Theta(z(t) - z'(t) - \frac{1}{v_h}|s(x, y) - s'|) \rho_{\text{rhomb}}(s', z'(t)), \quad (29)$$

where ρ_{rhomb} is defined by Eqs. (8) – (10). As before, we continue with $v_h = 1$.

ϕ_{rh} resembles ϕ_L in Eq. (11) which has the same source ρ_{rhomb} . However, unlike ϕ_L , ϕ_{rh} satisfies the Lentz differential equation, Eq. (6), *almost everywhere*.⁹ This was discussed in section (4.1). We refer to ϕ_{rh} as the “rhomboidal-source potential”, and distinguish it from ϕ_L which is also based on a rhomboidal source but uses a different defining equation.

The rhomboidal source $\rho_{\text{rh}}(s, z)$ is shown in Fig. (1) if coordinate x is replaced by coordinate s . The rhomboidal-source shift-vector components N_z^{rh} and N_x^{rh} , evaluated on slice $y = 0$, have the same values as N_z^L and N_x^L , as shown in Figs. (2) and (3) respectively.

In our opinion, ϕ_{rh} as defined in Eq. (29) is what Lentz intended in his study [31] instead of ϕ_L as defined in Eq. (11). These potential function definitions differ from one another in three ways.

- In the definition of ϕ_{rh} , we used s to force symmetry between x and y .
- ϕ_{rh} has an overall factor v_h whereas ϕ_L has a factor $1/v_h$. When $v_h = 1$ the distinction is hidden.
- The overall sign is different.

Before continuing, it is important to address the fact that, at certain values of (x, y, z) , the shift vector or its derivatives may be undefined. This is because the source function ρ_{rhomb} in Eq. (8), has regions of discontinuity (from the Heaviside function Θ) and the source function has an argument with discontinuous derivatives ($|x| + |y|$). At these discontinuities, derivatives

were undefined. The shift vector is initially defined only on the domain of points (x, y, z) , where the derivatives are well defined. We then extended the domain of the shift vector and its derivatives by defining them on the remaining points. This “extended” (also known as “completed”) shift vector isn’t unique. What does this mean physically? The true geometry of the universe is unlikely to have real mathematical discontinuities of the kind that appear in the Lentz warp drive. However, for the physical quantities computed in this study, all discontinuous behaviors are restricted to either step or delta functions, both of which can be treated as mathematical distributions. In particular, this implies that our results and analysis can be applied to any smooth geometry that matches ours outside of a proper-distance ϵ from the discontinuities. As for the interpolation region – i.e., the points within ϵ of the discontinuities – for sufficiently small ϵ , the integrated energy density will either approach 0 for a step-function discontinuity, or will have the same sign as the coefficient of the delta function. The planes $(x = 0)$, $(y = 0)$ are physically important because they form part of the domain of the discontinuities discussed above and ultimately lead to delta functions that contribute to the total energy density.

5.2 The energy

We now analyze the energy density of the ϕ_{rh} geometry and show that it violates the WEC. Along the way, we will show, using the ϕ_{rh} potential, some of the relationships discussed in the previous section on properties of HP warp drives.

Recall Eqs (16 – 18)

$$E = \frac{1}{8\pi} [T(x, y, z) + U(x, y, z)]$$

where, using Eq. (15) to expand $S(x, y, z)$

$$T(x, y, z) = 2(\delta(x) + \delta(y)) \partial_s \phi (\partial_s^2 \phi + \partial_z^2 \phi) + 4\delta(x)\delta(y) (\partial_s \phi)^2. \quad (30)$$

and

$$U(x, y, z) = (\rho(s, z) + 2\partial_z^2 \phi) \partial_z^2 \phi - 2(\partial_z \partial_s \phi)^2.$$

5.2.1 The U term

Lentz, in his Eq. (21), includes only the U term (Eq. (18)) in the energy inequality. He then concluded that the positivity of U implies the positivity of the energy density. Recall from Eq. (28) that

$$U(x, y, z) = \rho(s, z)\partial_z^2\phi + \alpha,$$

where $\alpha = 2\left((\partial_z^2\phi)^2 - (\partial_z\partial_s\phi)^2\right)$. α is positive if and only if ϕ_{rh} obeys the shift-derivative inequality, Eq. (24). If this would have been the case, then $U(x, y, z) \geq \rho(s, z)\partial_z^2\phi$. This result would be equivalent to that of Lentz's Eq. (13). However, we numerically demonstrate that the shift-derivative inequality fails. We portray this by plotting the term $|\partial_z^2\phi_{\text{rh}}| - |\partial_z\partial_s\phi_{\text{rh}}|$. It has regions of negativity, so the shift-derivative inequality fails. The results are shown in Fig. (6).

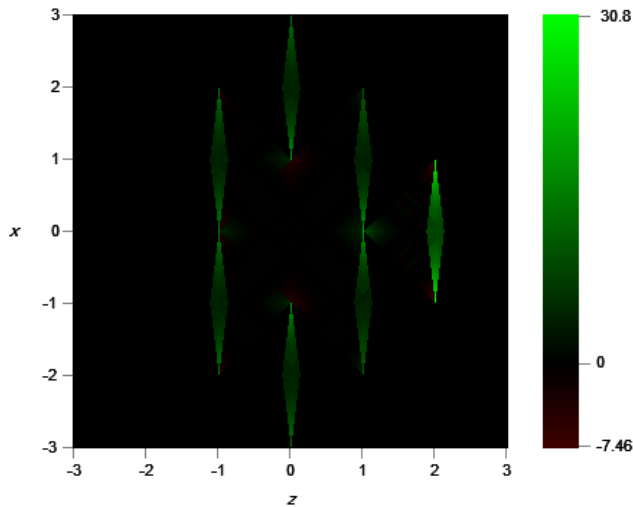


Figure 6: $|\partial_z^2\phi_{\text{rh}}| - |\partial_z\partial_s\phi_{\text{rh}}|$ for $y = 0$ (no γ -correction)

This image appears to show that the ϕ_{rh} obeys the shift-derivative inequality. However, we can see a hint of the small negative contributions. Therefore we replotted the function, but with γ set to 0.43, so that small negative values were sufficiently amplified to be visible.

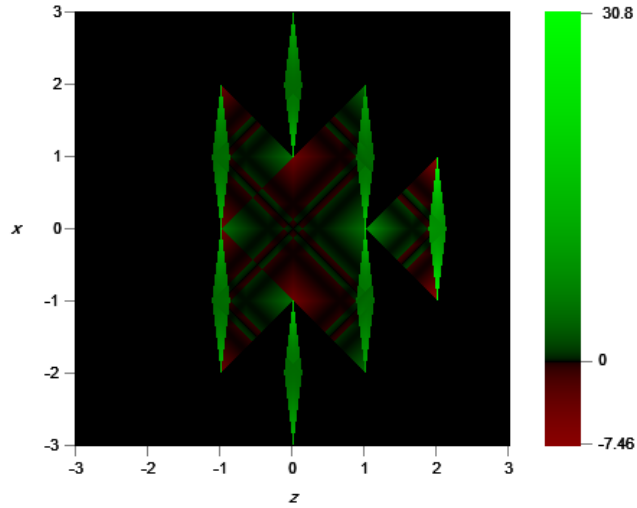


Figure 7: $|\partial_z^2 \phi_{\text{rh}}| - |\partial_z \partial_s \phi_{\text{rh}}|$ for $y = 0$ ($\gamma = 0.43$)

This new image clearly demonstrates the failure of the shift-derivative inequality for our rhomboidal-source geometry.

We have yet to consider the first term, $\rho(s, z)\partial_z^2 \phi$, on the RHS of Eq. (28). Even though the second term has regions of negativity, their values are small, so can, in principle, be easily compensated by large positive values of the first term. However, the term $\rho(s, z)\partial_z^2 \phi$ is displayed in Fig. 8 and can immediately be seen to have values ≤ 0 .

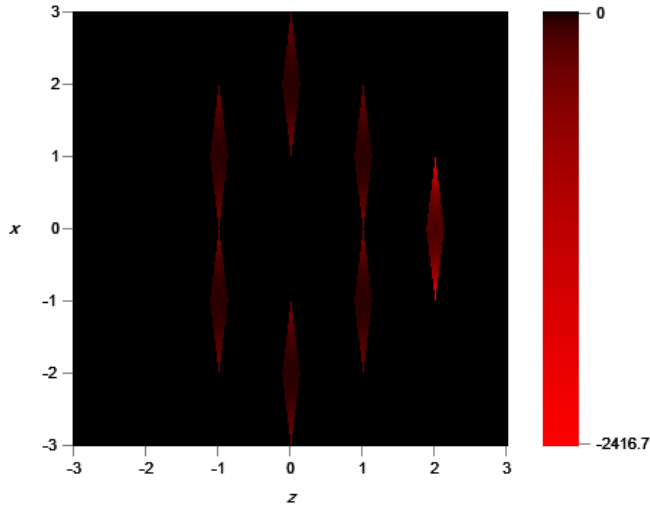


Figure 8: $\rho_{\text{rh}} \partial_z^2 \phi_{\text{rh}}$ for $y = 10^{-6}$ ($\gamma = 0.43$)

Note that this function has the opposite sign to that shown in Fig. 5 for Lentz’s original potential. These figures provide critical insights into the failure of Lentz’s demonstration of a WEC-compliant warp drive. Even if one was to set aside concerns about sets⁹ of measure 0 and the shift-derivative inequality, the key premise of Lentz’s demonstration was the non-negativity of $\rho_L \partial_z^2 \phi_L$. Owing to a sign mistake in the solution of his differential equation, Lentz incorrectly concluded that $\rho_L \partial_z^2 \phi_L \geq 0$.

It is possible that the modified potential ρ_{rh} (which solves Lentz’s differential equation almost everywhere) could have led to the same positivity as ρ_L , but as we can see from the figure, $\rho_{\text{rh}} \partial_z^2 \phi_{\text{rh}}$ is everywhere non-positive.

5.2.2 The T term

The energy density inequality in Eq. (16) includes the term T , given in Eq. (30). Formally, this term is irrelevant except for the singular planes $x = 0$ and $y = 0$. However, as previously mentioned, T should be understood as a distribution. This can be regarded as a (non-unique) approximation, where the δ functions are replaced by positive normalized spikes. In this case, note that the second term of $T(x, y, z)$ – namely, $4\delta(x)\delta(y) (\partial_s \phi)^2$ – is non-negative, albeit only near the singular line. On the other hand, the first term $2(\delta(x) + \delta(y))\partial_s \phi (\partial_s^2 \phi + \partial_z^2 \phi)$ need not be non-negative. To illustrate this,

we show in Fig. (9) the partial negativity of this term for our rhomboidal geometry.

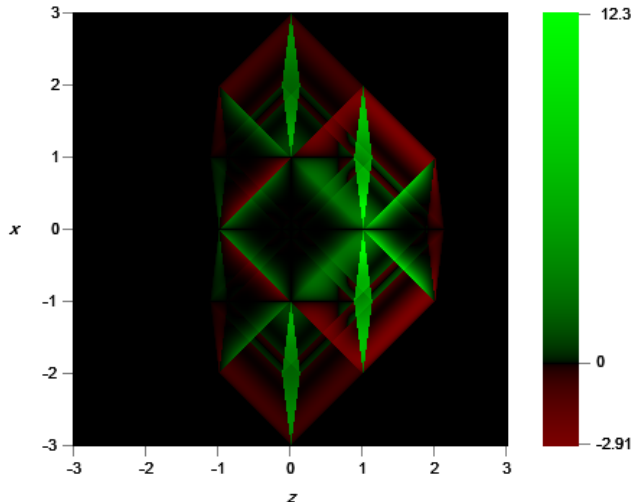


Figure 9: $\partial_s\phi_{\text{rh}} (\partial_s^2\phi_{\text{rh}} + \partial_z^2\phi_{\text{rh}})$ in the plane $x = 0$ ($\gamma = 0.5$)

In summary, $T(x, y, z)$ might be partially negative and thus, near the singular lines, the Eulerian energy density could become negative regardless of the values of U . We cannot ignore the singular regions just because of the delta functions. The WEC does not have a ‘singular-line exclusion.’

In fact, as we shall discuss further in the context of “no-go theorems,” the T term is essential for computing the total energy that is the integrated energy-density. Even though the energy density is ambiguous (owing to the options for completion of the singular planes), the integrated value (with unambiguous treatment of δ functions) is not. The total energy has a non-zero contribution from both T and U .

However, if the RHS has some regions of negativity – as it does for ϕ_{rh} (see Fig. 8)– then nothing can be concluded about the non-negativity of E .

5.2.3 Energy density

In summary, we have shown that both terms comprising the energy density term U have regions of negativity, and by comparing their respective figures,

we can easily see that their total (i.e., $U(x, y, z)$) also has regions of non-negativity. In particular, these regions are outside the critical planes $x = 0$ and $y = 0$ so cannot be compensated by the T term that we considered in Section 5.2.2.

In Fig. (10), we show the Eulerian energy density E_{rh} away from the critical planes, that is, we display $U(x, y, z)$ using Eq. 18. This appears to differ significantly from the Eulerian energy density based on ϕ_L , as shown in Fig. (4). Nevertheless, E_{rh} is also negative in some regions and thus, the ϕ_{rh} geometry also violates the Weak Energy Condition.

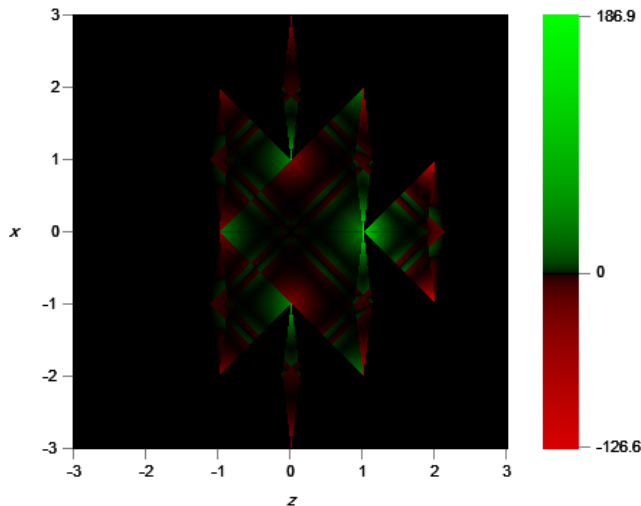


Figure 10: The Eulerian energy density E_{rh} for the rhomboidal source function at $y = 10^{-6}$ ($\gamma = 0.43$)

There is a significant difference between E_L and E_{rh} related to the discussion on energy density in Section 3.3. Computing E_L via (4) and (5) - the correct energy density corresponding to ϕ_L - reveals 45° bands that extend to infinity. Thus, the total energy of the ϕ_L warp-spacetime is infinite and therefore violates a key requirement of the geometry. This is a consequence of the fact that Lentz [31] defined ϕ_L as a function of a source that has incorrect arguments (see Appendix A.1) and, as a consequence, is not symmetric with respect to x and y . However, this is not the case for the ϕ_{rh} warp-spacetime, for which the energy is bounded. This can be proven from the fact that the rhomboidal source (with the correct arguments) satisfies the three conditions of Subsection 4.3. The last two conditions (source-domain

boundedness and $s(x, y) = |x| + |y|$) are satisfied trivially. To demonstrate the cancellation condition, consider the seven rhomboidal (sub)domains of the source function. Any diagonal line either intersects no rhomboids or intersects rhomboids whose weights add up to 0 and whose intersection line-segments are identical to one another relative to their respective rhomboid centroids.

There is also a significant difference between the Eulerian energy densities in Fig. 3 in ref. [31] and E_{rh} . This is because computing E_L using Lentz's Eq. (17) yields a completely different result than that obtained using Eqs. (4) and (5), respectively. Note that computing E_{rh} using Eq. (16) with $U(x, y, z)$ given by Eq. (18), which is equivalent to Lentz's Eq. (17) away from the critical planes, yields the same result as obtained using Eqs. (4) and (5), respectively. This distinction is made because ϕ_{rh} is a solution of Lentz's hyperbolic differential equation, whereas ϕ_L is not.

6 Analysis of a rectangular-source HP warp drive

Next, we next consider a slight modification of the Lentz source function. Instead of a collection of rhomboids, we take the source to consist of a collection of rectangles.¹²

$$\rho_{\text{rect}}(s, z) = \tilde{\rho}_{\text{rect}}(x, y, z) = W \sum_{i=1}^4 \tilde{\alpha}_i \Theta(p_{1,i}(z)) \Theta(p_{2,i}(s)) g_i(s), \quad (31)$$

where

$$\begin{aligned} p_{1,i}(z) &= \tilde{L}_z - |z - \xi_i|, \\ p_{2,i}(s) &= \tilde{L}_x - ||s| - \beta_i|, \\ g_i(s) &= Q_{\text{max}}. \end{aligned} \quad (32)$$

where after substituting rectangles for rhomboids, the parameter descriptions and values are the same as those described for the rhomboidal sources in Section 3.2, except that the minimum charge Q_{min} is not relevant. The constraints on the overall source configuration are also the same.

¹²Although function $g_i(s)$ presented in Eq. (31) may seem trivial, it is provided so that equation fits the general scheme presented in Appendix C.

The unscaled rectangular source is displayed in Fig.(11). That is, we show $\rho_{\text{rect}} N_z^{\text{rect}}(0, 0, 0)$, for an easy comparison with the unscaled rhomboidal source shown in Fig. 1.

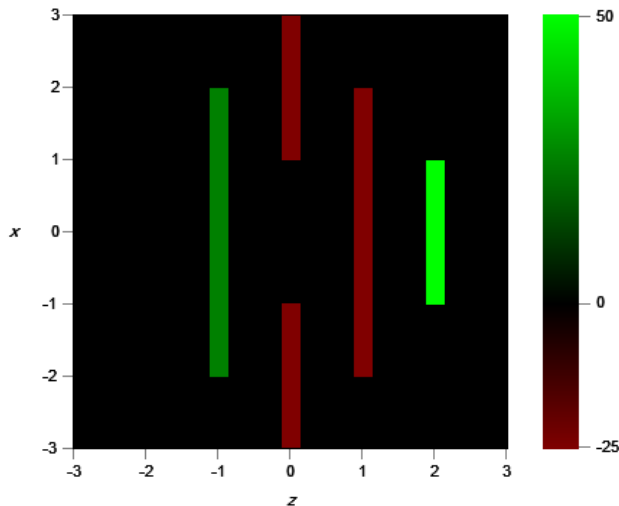


Figure 11: Unscaled rectangular source $\rho_{\text{rect}} N_z^{\text{rect}}(0, 0, 0)$

Similarly to Eq. (29), we obtain the shift-vector potential ϕ_{rect} .

$$\phi_{\text{rect}}(x, y, z(t)) = -\frac{1}{4} \int_{-\infty}^{\infty} dx' dz' \Theta(z(t) - z' - |x - x'|) \rho_{\text{rect}}(s', z'), \quad (33)$$

where $z(t) = z - vt$, v is the speed of the warp drive, and ρ_{rect} is defined by Eqs. (31) – (32). Recall that $s(x, y) = |x| + |y|$ and $\rho(s(x, y), z) = \rho(-s(x, y), z) = \tilde{\rho}(x, y, z)$. As in the rhomboidal case, we have a slight abuse of notation, and set $\phi_{\text{rect}}(s, z) = \phi_{\text{rect}}(x, y, z)$.

As mentioned in Section 3.2, the warp drive based on rectangular sources is superior to that based on rhomboidal sources, in the sense that N_z^{rect} is non-zero and precisely level, and N_x^{rect} and N_y^{rect} are precisely zero over a broader central region. This is illustrated in Fig. 12, which shows the comparative profiles of N_z^{rect} and N_z^{rhomb} , along the z -direction at $(x, y) = (0, 0)$, and in Fig. 13, which shows the comparative profiles of N_x^{rect} and N_x^{rhomb} , also along the z -direction, but at $(x, y) = (-0.2, 0)$.

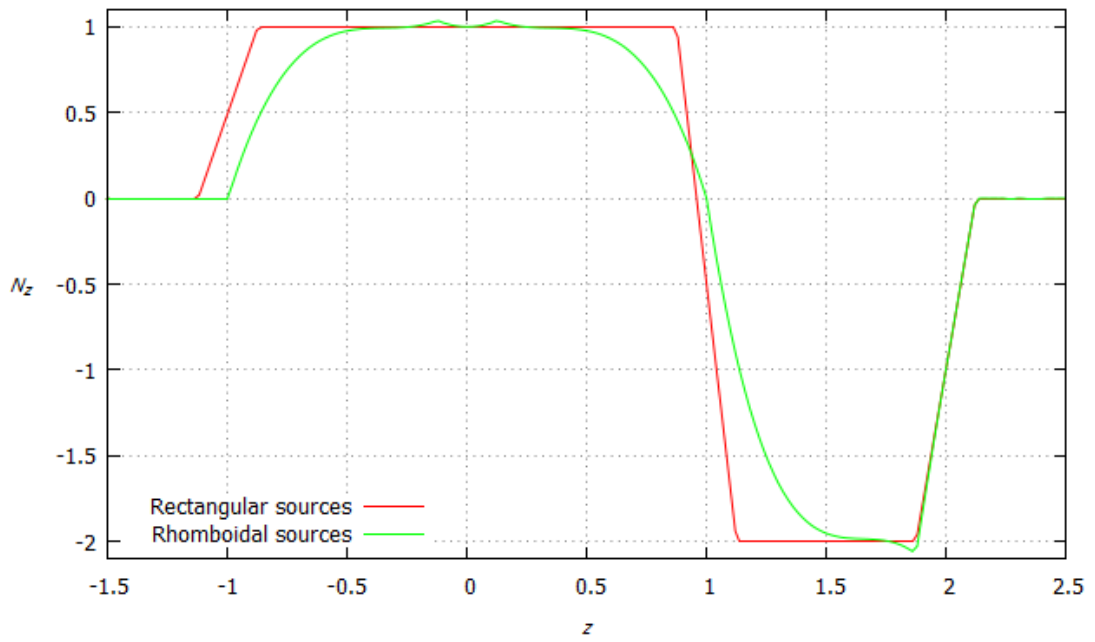


Figure 12: Comparative profiles of $N_z^{\text{rect}}(x, y, z)$ and $N_z^{\text{rhomb}}(x, y, z)$ at fixed $(x, y) = (0, 0)$.

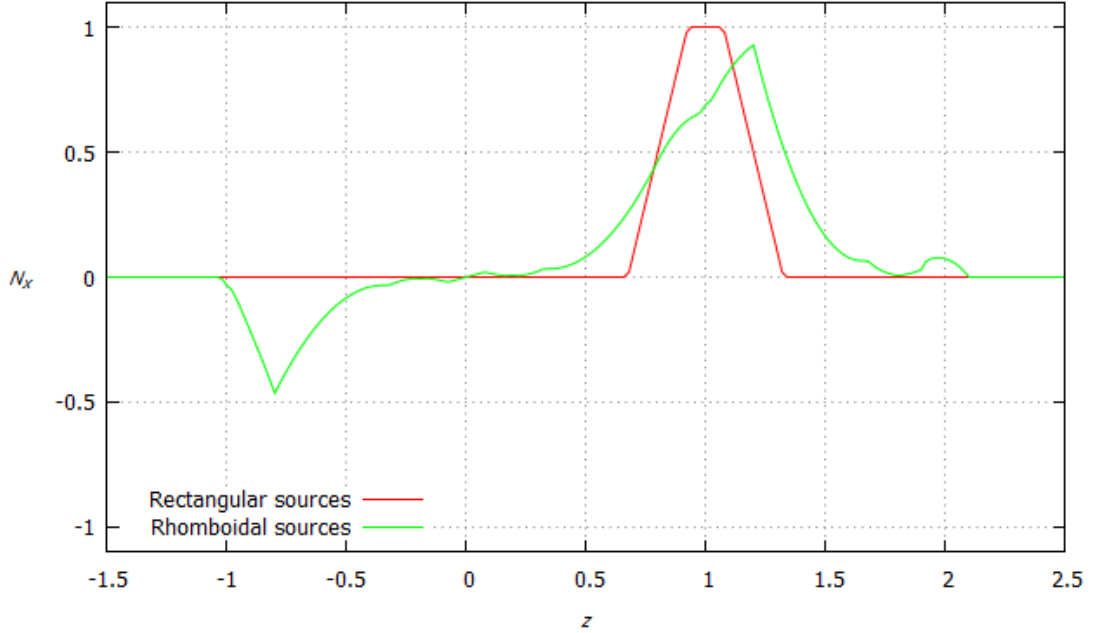


Figure 13: Comparative profiles of $N_x^{\text{rect}}(x, y, z)$ and $N_x^{\text{rhomb}}(x, y, z)$ at fixed $(x, y) = (-0.2, 0)$.

Does the resultant warp-drive geometry have a positive WEC? We will briefly see by direct computation that this does not occur. First, let us examine what we would expect based on Lentz's inequality analysis. Recall the argument in section 4.4, that if $T_{\text{rect}}(x, y) + \rho_{\text{rect}} \partial_z^2 \phi_{\text{rect}}$ were positive (where $T_{\text{rect}}(x, y)$ is zero almost everywhere), then the energy density would be positive. We observed that this conclusion hinges on the validity of the shift-derivative inequality. However, that inequality turns out to be irrelevant (just as in the rhomboidal case) because, as shown in Fig. (14), $\rho_{\text{rect}} \partial_z^2 \phi_{\text{rect}}$ is negative in the rectangular regions where the source is non-zero.

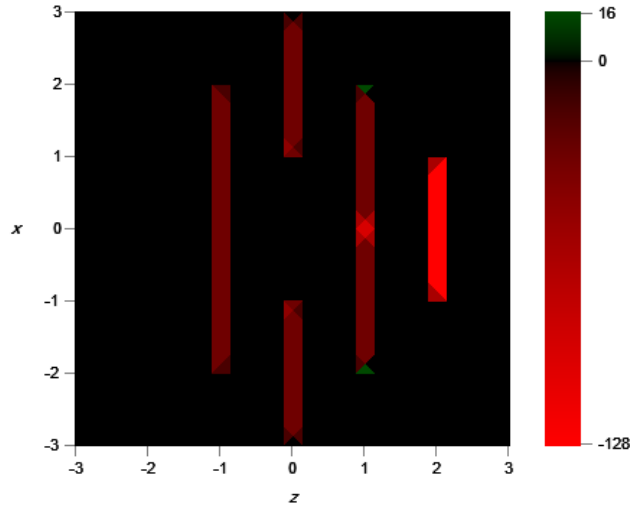


Figure 14: $\rho_{\text{rect}} \partial_{\mathbf{z}}^2 \phi_{\text{rect}} (\gamma = 0.60)$

What we have demonstrated thus far, is that the rectangular-source geometry doesn't meet the requirements of Lentz's modified energy inequality theorem for proving non-negativity of the Eulerian energy density, not even approximately. Of course, it could still happen "accidentally" that the Eulerian energy density turns out to be non-negative. In Fig. (15) we show the Eulerian energy density E_{rect} computed using Eq. (18). As for the rhomboidal-source example, it is negative in some regions and thus violates the Weak Energy Condition. It is noteworthy that, unlike the rhomboidal-source example, the energy-density is zero except in a few small regions. However, we don't see how to modify the sources to eliminate regions of negative energy-density altogether. Also, even if we could find such sources, we would need to separately examine the contribution of T which could turn out to be negative.

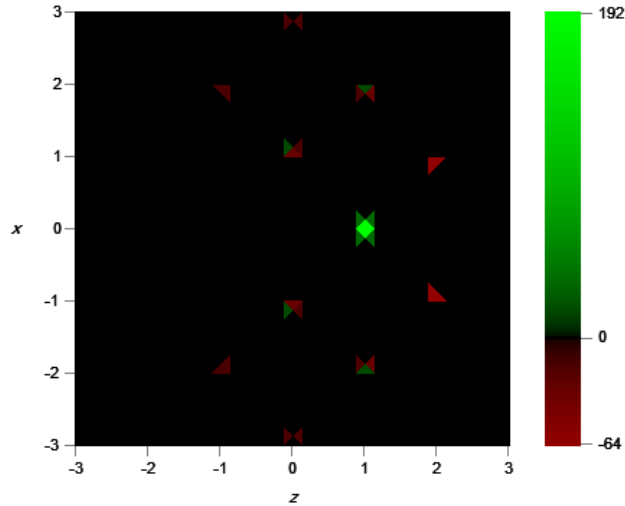


Figure 15: The Eulerian energy density E_{rect} for the rectangular source function ($\gamma = 0.50$)

7 Applicability of no-go theorems to Lentz-style warp drives

In this study, we address an apparent paradox in the literature. On the one hand, there are “no-go” theorems stating that Natario warp drives must violate various energy conditions, such as the WEC. On the other hand, there is an example, proposed by Lentz, of a Natario warp drive that supposedly has been demonstrated to satisfy the WEC. There are only three possible ways to resolve this paradox:

1. The no-go theorems are wrong.
2. The Lentz demonstration is wrong.
3. Lentz’s warp drive does not satisfy the conditions required for the no-go proofs.

Unfortunately, lacking a resolution to this issue, there has continued to be murkiness about whether a WEC-compliant Natario warp drive can be constructed.

It was tempting to assume no errors either in the no-go proofs or in Lentz’s demonstration, and to focus instead on whether Lentz’s warp drive satisfies the assumptions of the no-go theorems. However, it has turned out that this level of subtlety is unnecessary. Lentz’s demonstration is incorrect. Hence, the paradox is resolved: no Natario warp-drive has been demonstrated to comply with the WEC. Hopefully, this conclusion will help dispel the murkiness of the status of the Lentz drive.

There is still the question of whether one can create a Natario warp drive by relaxing any of the conditions of the no-go theorems. In particular, we considered the theorems of Santiago et al. [20]. In Section 7.4, the authors proved that a Natario warp-drive must violate the WEC. The authors derived, for a 0-vorticity warp drive (such as the Lentz warp drive) (Eq. 7.12 of ref. [20]), the Eulerian energy density E satisfies $E = \partial_i \mathcal{S}_i = 0$ where $\mathcal{S}_i = \frac{1}{16\pi} (N_i \partial_j N_j - N_j \partial_i N_j)$. From Stoke’s theorem, $\int d^3x E = 0$, provided that \mathcal{S}_i falls off quickly enough so that integral of \mathcal{S}_i is 0 on the surface at infinity. From this, we see that the energy density is either precisely zero everywhere or must have some regions of negativity (of equal weight to regions of positivity), hence violating the WEC.

Note that if \mathcal{S} were to fall off quadratically, then the boundary-integral would be non-zero and the total energy would be finite. Finiteness is important because we would still have a physically meaningful theory, but the above WEC-violation proof would fail. Unfortunately, WEC compliance cannot be established simply by showing non-negativity of the Eulerian energy density. One must show the non-negativity of the energy density for **any** reference frame. One way to do this, as argued in Ref. [20], is to show that in addition to the non-negativity of the Eulerian energy density, there is also non-negativity of a second parameter which is the sum of the average Eulerian pressure and Eulerian energy density. The authors prove in their section 7.4 (in the discussion of the Null Energy Condition) that this second parameter must have some regions of negativity. This proof does not appear to depend on the rapid spatial fall-off of \mathcal{S}_i . However, the proof requires an additional (physically motivated) assumption: the warp drive must be turned on at large negative times and turned off at large positive times. We refer to this as the “on-off condition.”

In summary, Santiago et al. [20] proved that the WEC is violated provided that \mathcal{S}_i falls off quickly enough or that the warp drive satisfies the on-off condition.¹³ If we are willing to relax these conditions, then it might be possible

¹³Santiago et al. [20] prove that the on-off condition implies NEC violation, which implies

to construct a WEC-compliant Natario warp drive. It should be emphasized that we did not find such a warp drive (although we have investigated a Fell-Heisenberg drive [35] with a positive Eulerian density, which nevertheless violates the WEC), nor have we proven that such a WEC-compliant drive can be constructed.

7.1 Validity of Stoke's theorem for ϕ_{rh} and ϕ_{rect}

There is one more set of assumptions implicit in the above theorems, which are not satisfied by Lentz's warp drive or the variants explored in this paper. These assumptions have to do with the smoothness of the geometric parameters, a quality we expect from physical theories. The proposals we explored all had regions where the shift vector was not differentiable. This lack of differentiability could, in principle, render the theorems (for example, Stoke's theorem) invalid and could therefore provide a loophole that would allow WEC-compliance. One reason we have gone through the computation and analysis of the Lentz warp drives, is to determine whether there may be a possible role of non-differentiability in the non-applicability of the no-go theorems.

The Stokes'-based no-go proof is probably valid despite the lack of differentiability of the ϕ_{rh} and ϕ_{rect} geometries. To observe this, we computed the total energy E_{TOT} for both geometries, where from Eq. (16),

$$E_{\text{TOT}} = \frac{1}{8\pi} \int dx dy dz (T(x, y, z) + U(x, y, z)). \quad (34)$$

See Appendix E for details on how to integrate the T term.

Because our goal is to compare the total energy to 0, we need to scale the energy-density by a constant $1/E_{\text{scale}}$, which we define as

$$E_{\text{scale}} = \int dx dy dz (|T(x, y, z)| + |U(x, y, z)|). \quad (35)$$

(Note that because T involves the absolute values of δ -functions, we adopt the definition that $|\delta(x)| \equiv \delta(x)$.) As an example, we numerically computed using a grid with 300 steps in each direction, $E_{\text{TOT}}^{\text{rh}}/E_{\text{scale}}^{\text{rh}} \approx 0.034$. This calculation was numerically consistent with a total energy of 0. For

WEC violation.

better numerical accuracy, we must increase n – the number of grid steps in each direction. In Figs. 16 and 17, we show the scaled total rhomboidal geometry and rectangular geometry energies as a function of n . The graphs are consistent with the convergence to $E_{\text{TOT}} = 0$.

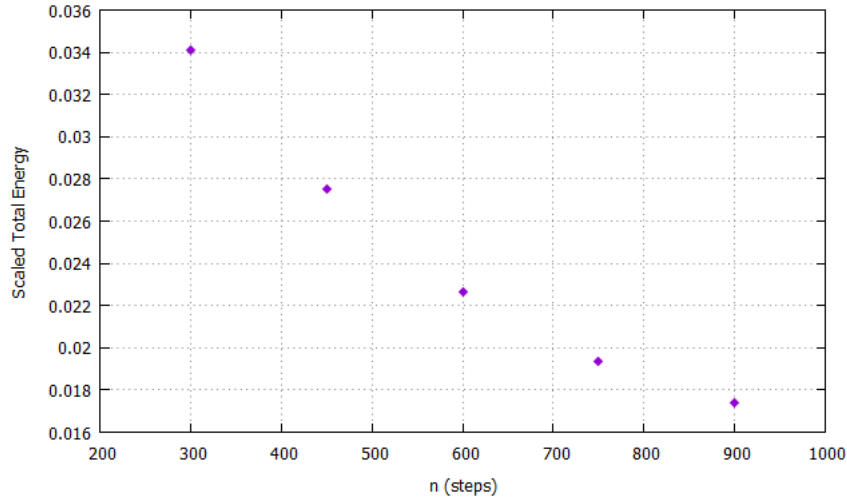


Figure 16: $\frac{E_{\text{TOT}}^{\text{rh}}}{E_{\text{scale}}^{\text{rh}}}$ as a function of n for the rhomboidal source function.

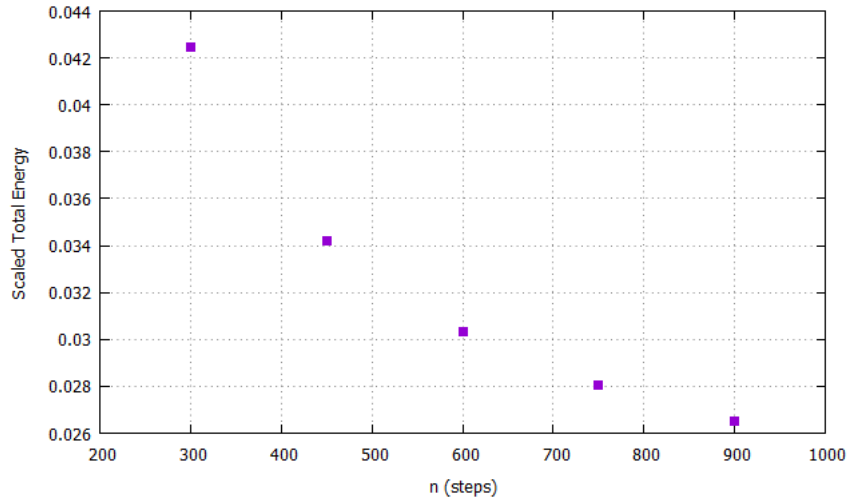


Figure 17: $\frac{E_{\text{TOT}}^{\text{rect}}}{E_{\text{scale}}^{\text{rect}}}$ as a function of n for the rectangular source function.

8 Conclusions

In ref. [31], Lentz proposed a new warp-drive geometry claimed to be WEC compliant. In this study, we showed that this claim is incorrect. The Lentz warp drive violates the WEC. We have shown this directly by the numerical computation of the energy density, as shown in Fig. 4. We also found and explained various errors made by Lentz in his computations, as well as in the development of his theoretical requirements for the construction of a WEC-compliant warp drive.

None of this should be surprising, given that there are no-go theorems discussed in Section 7, which state the impossibility of WEC-compliant warp drives. Of course, similar to all theorems, there are assumptions and conditions. These include the differentiability requirements violated by Lentz's geometry.

We also explored whether Lentz's proposal and implementation could be modified to achieve the desired result. We were able to test a couple of geometric models that were similar to Lentz's but that corrected some of the original errors. Unfortunately, these violate the WEC as well.

In the last section, we discuss the applicability of various no-go theorems to warp drives presented in this study. Our modified rhomboidal and rectangular warp drives satisfy the rapid-falloff condition of the no-go theorem for Eulerian energy, but not the on-off condition or the differentiability condition. However, despite these possible no-go loopholes, the Lentz and modified Lentz warp drives violate the WEC, as we have shown.

A Derivation of the Hyperbolic Potential

In Section 5, we introduce a modified version of Lentz's potential given by Eq. (29), and we then generalize this for general source functions ρ , to Eq. (12). This potential is referred to as the hyperbolic potential (HP). We then re-introduce v_h which had earlier been set as $v_h = 1$, and obtain

$$\phi(x, y, z) = -\frac{1}{4}v_h \int_{-\infty}^{+\infty} \int_{-\infty}^{+\infty} ds' dz' \Theta(z - z' - \frac{1}{v_h}|s - s'|) \rho(s', z'), \quad (36)$$

where it is implicit that z is a function of t and $s = |x| + |y|$. We demonstrate via Eq. (15), that when $v_h = 1$, ϕ is a solution of Eq. (6) everywhere except

for the planes $x = 0$ and $y = 0$. This is also the case for general values of v_h . Next, we explain how we obtain Eq. (36) as a solution to Lentz's hyperbolic differential equation Eq.(6) , which is repeated here for convenience.

$$\partial_x^2 \phi + \partial_y^2 \phi - \frac{2}{v_h^2} \partial_z^2 \phi = \rho, \quad (37)$$

(where the tildas are removed). If we now require that

$$\phi(x, y, z) = \phi(s(x, y), z), \quad (38)$$

it can be shown that, by applying the chain rule to (38) and performing some algebra, that, if $x, y \neq 0$ and $s = |x| + |y|$, then

$$\partial_x^2 \phi = \partial_y^2 \phi = \partial_s^2 \phi, \quad (39)$$

where, from this point forward, we exclude $x = 0$ and $y = 0$ from the domain of ϕ . We may then rewrite Eq. (37) as

$$2\partial_s^2 \phi - \frac{2}{v_h^2} \partial_z^2 \phi = \rho. \quad (40)$$

Then, by multiplying both sides of Eq. (40) by $-2/v_h^2$ and rearranging, we obtain

$$\partial_z^2 \phi - v_h^2 \partial_s^2 \phi = -\frac{v_h^2}{2} \rho. \quad (41)$$

The preceding equation is readily recognized as a 1-dimensional wave equation, written canonically as

$$\partial_t^2 \phi - v^2 \partial_s^2 \phi = f \quad (42)$$

with the identification

$$\begin{aligned} t &= z \\ v^2 &= v_h^2 \\ f &= -\frac{v_h^2}{2} \rho. \end{aligned} \quad (43)$$

ϕ can therefore be written as

$$\phi(t, s) = \int_{-\infty}^{+\infty} \int_{-\infty}^{+\infty} dt' ds' G(t - t', s - s') f(t', s') \quad (44)$$

where G is the Green's function given by

$$G(t, x) = \frac{1}{2v} \Theta \left(t - \frac{|s|}{v} \right) \quad (45)$$

Then the corresponding solution to Eq. (42) is given by

$$\phi = \int_{-\infty}^{+\infty} \int_{-\infty}^{+\infty} dt' ds' \frac{1}{2v} \Theta \left(t - t' - \frac{|s - s'|}{v} \right) f(t', s'). \quad (46)$$

Then, substituting Eqs. (43) into Eq. (46) yields

$$\phi = \int_{-\infty}^{+\infty} \int_{-\infty}^{+\infty} dz' ds' \frac{1}{2v_h} \Theta \left(z - z' - \frac{1}{v_h} |s - s'| \right) \left(-\frac{v_h^2}{2} \rho(s', z') \right) \quad (47)$$

which simplifies to

$$\phi = -\frac{1}{4} v_h \int_{-\infty}^{+\infty} \int_{-\infty}^{+\infty} dz' ds' \Theta \left(z - z' - \frac{1}{v_h} |s - s'| \right) \rho(s', z') \quad (48)$$

and we can observe that the RHS of Eq. (48) is identical to that of Eq. (36).

A.1 Why Lentz's original potential is not a hyperbolic potential

Eq. 48 can be compared with Lentz's original potential, given by eq. (11) and is repeated for convenience.

$$\phi_L = \frac{1}{4v_h} \int_{-\infty}^{\infty} dx' dz' \Theta \left(z - z' - \frac{1}{v_h} |x - x'| \right) \rho(|x'| + |y|, z') \quad (49)$$

Eq. (49) exhibits the following differences, relative to Eq. (48):

- An overall sign that is positive instead of negative.
- An overall factor is $1/v_h$ instead of v_h .
- A factor $|x - x'|$ instead of $|s - s'|$, in the argument to Θ .

- The expression $|x'| + |y|$ instead of s' , as in the second argument to ρ .

The incorrectness in Eq. (49) can be obtained numerically. Recall that we have two methods for computing the Eulerian energy density: 1) via Lentz's Eq. (17), which requires ϕ to be a solution of Eq. (37); and 2) via Eqs. (4) and (5), which is correct regardless. The images of the Eulerian energy density derived from (48) via method 1 are identical (other than possibly on the lines $x = 0$ or $y = 0$) to those obtained from Eq. (48) using method 2. The same cannot be said for Eq. (49). In particular, the sign error (first bullet, above) directly leads to the incorrect image, as shown in Fig. 3, in Ref. [31], which demonstrates that the WEC is satisfied. That is, if we begin with Eq. (48) and only change sign, the image (without γ -correction) of Eulerian energy density near $y = 0$, as obtained via method 1, is qualitatively the same erroneous result, that is, different from the correct result obtained via method 2, as shown in Lentz's [31] Fig. (3).

The last two bullets imply that Eq. (49) is inconsistent with Lentz's prescription that $s = |x| + |y|$. These errors lead to violations of the boundedness requirement for the shift vector components and Eulerian energy density, and thus to infinite energy. This is not the case for the potential in Eq. (48). Furthermore, the asymmetry between x and y means that $\partial_x^2 \phi \neq \partial_y^2 \phi$. (See Appendix H for a discussion of $\partial_y^2 \phi$.) The equality of these two 2nd-order partial derivatives is a vital step, i.e. Eq. (39), to derive the potential: because the equality does not hold in this case, the original differential equation (37) does not reduce to Eq. (41) and thus cannot be identified with the 1-dimensional wave equation (42); therefore, Eq. (49) cannot be a solution to Eq. (37).

B Derivation of the expressions for the shift vector components

The shift vector components are presented in Eq. (25) and repeated below for convenience, except that, for greater generality, we do not assume that $v_h = 1$:

$$N_z = \partial_z \phi = -\frac{1}{4} v_h \int_{-\infty}^{\infty} ds' \rho(s', z - v_h^{-1} |s - s'|) \quad (50)$$

$$N_x = \partial_x \phi = \text{sgn}(x) \partial_s \phi = \frac{1}{4} \text{sgn}(x) \int_{-\infty}^{\infty} ds' \text{sgn}(s-s') \rho(s', z - v_h^{-1} |s-s'|) \quad (51)$$

$$N_y = \partial_y \phi = \text{sgn}(y) \partial_s \phi = \frac{1}{4} \text{sgn}(y) \int ds' \text{sgn}(s-s') \rho(s', z - v_h^{-1} |s-s'|) \quad (52)$$

The first two equations are derived in Appendix B.1 and the integral that appears in the last of these equations is derived in Appendix B.2.

B.1 Derivation of N_z

In deriving N_z , we will make use of the following identities:

$$\partial_u \Theta(q(u, w, \dots)) \equiv \delta(q(u, w, \dots)) \partial_u q \quad (53)$$

and

$$\int_{-\infty}^{\infty} \delta(q(u, w, \dots)) f(u, w, \dots) du \equiv \sum_i \frac{f(r_i, w, \dots)}{|\partial_u q|_{u=r_i}} \quad (54)$$

where r_i is the i th root of $q(u, w, \dots) = 0$, treating q as a function of u , only. Analogous equations hold for variables w , etc.

As $N_z = \partial_z \phi$, where ϕ is given by Eq. (48), we can differentiate Eq. (48) with respect to z ,

$$N_z = -\frac{1}{4} v_h \int_{-\infty}^{\infty} \left[\int_{-\infty}^{\infty} \partial_z \Theta(z - z' - v_h^{-1} |s - s'|) \cdot \rho(s', z') dz' \right] ds'. \quad (55)$$

Thus, we must evaluate the derivative $\partial_z \Theta(z - z' - v_h^{-1} |x - x'|)$. To this end, we define

$$q(s, s', z, z') = z - z' - v_h^{-1} |s - s'| \quad (56)$$

so we have $\partial_z q = 1$. Then, applying the identity (53), we obtain

$$\partial_z \Theta(q(s, s', z, z')) = \delta(q(s, s', z, z')) \partial_z q = \delta(q(s, s', z, z')) \quad (57)$$

and, substituting Eq. (57) into Eq. (55), we have

$$N_z = -\frac{1}{4}v_h \int_{-\infty}^{\infty} \left[\int_{-\infty}^{\infty} \delta(q(s, s', z, z')) \rho(s', z') dz' \right] ds'. \quad (58)$$

Then, by applying identity (54) to the inner integral of Eq. (58), we have

$$\int_{-\infty}^{\infty} \delta(q(s, s', z, z')) \rho(s', z') dz' = \sum_i \frac{\rho(s', r_i)}{|\partial_{z'} q|_{z'=r_i}}, \quad (59)$$

where, in this case, from Eq. (56), we have $\partial_{z'} q = -1$ and setting $q(s, s', z, z') = 0$ and solving for z' yields one root, that is

$$r_1 = z - v_h^{-1}|s - s'|. \quad (60)$$

Therefore, there is only one term in the summation of the RHS of Eq. (59). Thus, Eq. (59) becomes

$$\int_{-\infty}^{\infty} \delta(q(s, s', z, z')) \rho(s', z') dz' = \frac{\rho(s', r_1)}{|-1|} = \rho(s', z - v_h^{-1}|s - s'|) \quad (61)$$

and substituting this result into Eq. (58), we have

$$N_z = -\frac{1}{4}v_h \int_{-\infty}^{\infty} \rho(s', z - v_h^{-1}|s - s'|) ds'. \quad (62)$$

and we see that Eq. (62) is identical to Eq. (50).

B.2 Derivation of N_x and N_y

Because know $N_x = \partial_x \phi = \text{sgn}(x) \partial_s \phi$ and $N_y = \partial_y \phi = \text{sgn}(y) \partial_s \phi$, we only need to obtain the correct expression for $\partial_s \phi$, where ϕ is again given by Eq. (48). In other words, we differentiate Eq. (48) w.r.t. s , to obtain

$$\partial_s \phi = -\frac{1}{4}v_h \int_{-\infty}^{\infty} \left[\int_{-\infty}^{\infty} \partial_s \Theta(z - z' - v_h^{-1}|s - s'|) \cdot \rho(s', z') ds' \right] dz'. \quad (63)$$

Let us first reverse the order of integration, i.e.

$$\partial_s \phi = -\frac{1}{4} v_h \int_{-\infty}^{\infty} \left[\int_{-\infty}^{\infty} \partial_s \Theta(z - z' - v_h^{-1} |s - s'|) \cdot \rho(s', z') dz' \right] ds'. \quad (64)$$

Again, taking q to be defined in Eq. (56), we have

$$\partial_s q = -v_h^{-1} \text{sgn}(s - s'). \quad (65)$$

Then, applying identity (53), we obtain

$$\partial_s \Theta(q(s, s', z, z')) = \delta(q(s, s', z, z')) \partial_s q = -v_h^{-1} \text{sgn}(s - s') \delta(q(s, s', z, z')) \quad (66)$$

and substituting Eq. (66) into Eq. (64), we have

$$\partial_s \phi = \frac{1}{4} \int_{-\infty}^{\infty} \text{sgn}(s - s') \left[\int_{-\infty}^{\infty} \delta(q(s, s', z, z')) \rho(s', z') dz' \right] ds'. \quad (67)$$

Then, applying identity (54) to the inner integral of Eq. (67), we obtain the same result as Eq. (61), because z' is - once again - the integration variable. Then, substituting Eq. (61) into Eq. (67), we have

$$\partial_s \phi = \frac{1}{4} \int_{-\infty}^{\infty} \text{sgn}(s - s') \rho(s', z - v_h^{-1} |s - s'|) ds', \quad (68)$$

and we see that Eq. (68) is consistent with Eqs. (51) and (52).

C Analytic evaluation of integrals

This appendix describes the algorithm used to evaluate the integrals in Eqs. (62) and (68), each of which contains the function $\rho(s', z')$. For the source functions presented in this paper, $\rho(s', z')$ takes the general form

$$\rho(s', z') = W \sum_{i=1}^4 \alpha_i \left[\prod_{\sigma} \Theta(p_{\sigma, i}(s', z')) \right] g_i(s'), \quad (69)$$

where:

- Θ is the Heaviside function.
- The set of $p_{\sigma,i}$ is a family of *shape functions*, where
 - The index σ runs over a number of expressions, which together determine the source geometry, for example, rhomboids or rectangles.
 - The index i runs over the centroids (β_i, ξ_i) of that geometry.
- Set g_i is a family of *charge profiles* that determines the charge as a function of the distance from β_i .
- The functions $p_{\sigma,i}$ and g_i are continuous, but not necessarily smooth.
- $z' = z - v_h^{-1}|s - s'|$, as shown in Eqs. (62) and (68).

The specific shape function(s) and charge profile for each of the rhomboidal and rectangular sources are presented in Subsections C.1 and C.2.

We will now continue with the general case. From Eq. (50) we write

$$\partial_z \phi = -\frac{1}{4} v_h W \sum_{i=1}^4 \alpha_i \mathcal{I}_{1,i}(s, z) \quad (70)$$

and from Eq. (51) or (52) we write

$$\partial_s \phi = \frac{1}{4} W \sum_{i=1}^4 \alpha_i \mathcal{I}_{2,i}(s, z), \quad (71)$$

where

$$\mathcal{I}_{1,i}(s, z) = \int_{-\infty}^{\infty} \left[\prod_{\sigma} \Theta(p_{\sigma,i}(s', z - v_h^{-1}|s - s'|)) \right] g_i(s') ds' \quad (72)$$

and

$$\mathcal{I}_{2,i}(s, z) = \int_{-\infty}^{\infty} \frac{s - s'}{|s - s'|} \left[\prod_{\sigma} \Theta(p_{\sigma,i}(s', z - v_h^{-1}|s - s'|)) \right] g_i(s') ds'. \quad (73)$$

At a fixed point (s, z) , the functions $p_{\sigma,i}(s', z - v_h^{-1}|s - s'|)$ are piece-wise linear in s' , crossing $p_{\sigma,i}(s', z - v_h^{-1}|s - s'|) = 0$ a finite number of times, where $p_{\sigma,i}(s', z - v_h^{-1}|s - s'|) < 0$ if s' is less than the smallest root or greater than the largest root. On the open s' -interval between any pair of consecutive roots, a particular $p_{\sigma,i}(s', z - v_h^{-1}|s - s'|)$ is either negative or positive. If it happens that, for fixed i , $p_{\sigma,i}(s', z - v_h^{-1}|s - s'|) > 0$ for all σ , then $\prod_{\sigma} \Theta(p_{\sigma,i}(s', z - v_h^{-1}|s - s'|)) = 1$; otherwise $\prod_{\sigma} \Theta(p_{\sigma,i}(s', z - v_h^{-1}|s - s'|)) = 0$. Thus, for each i , there exists, at most, a finite number of open intervals $I_{i,k}^+ = (a_{\sigma_a,i,k}, b_{\sigma_b,i,k})$ ¹⁴ that contribute to integrals $\mathcal{I}_{1,i}$ and $\mathcal{I}_{2,i}$. Based on this analysis, integrals $\mathcal{I}_{1,i}$ and $\mathcal{I}_{2,i}$ can be rewritten as a finite sum of finite integrals (rather than improper integrals), where the interval bounds become the limits of integration. That is,

$$\mathcal{I}_{1,i}(s, z) = \sum_k \int_{a_{\sigma_a,i,k}}^{b_{\sigma_b,i,k}} g_i(s') ds' \quad (74)$$

$$= \sum_k A_i(b_{\sigma_b,i,k}) - A_i(a_{\sigma_a,i,k}) \quad (75)$$

and

$$\mathcal{I}_{2,i}(s, z) = \sum_k \begin{cases} \int_{a_{\sigma_a,i,k}}^{b_{\sigma_b,i,k}} g_i(s') ds', & s > b_{\sigma_b,i,k} \\ - \int_{a_{\sigma_a,i,k}}^{b_{\sigma_b,i,k}} g_i(s') ds', & s < a_{\sigma_a,i,k} \\ \int_{a_{\sigma_a,i,k}}^s g_i(s') ds' - \int_s^{b_{\sigma_b,i,k}} g_i(s') ds', & a_{\sigma_a,i,k} < s < b_{\sigma_b,i,k} \end{cases} \quad (76)$$

$$= \sum_k \begin{cases} A_i(b_{\sigma_b,i,k}) - A_i(a_{\sigma_a,i,k}), & s > b_{\sigma_b,i,k} \\ A_i(a_{\sigma_a,i,k}) - A_i(b_{\sigma_b,i,k}), & s < a_{\sigma_a,i,k} \\ 2A_i(s) - A_i(a_{\sigma_a,i,k}) - A_i(b_{\sigma_b,i,k}), & a_{\sigma_a,i,k} < s < b_{\sigma_b,i,k} \end{cases} \quad (77)$$

respectively, where:

- The quantity A_i denotes an antiderivative of g_i .
- The factor $\frac{s-s'}{|s-s'|}$, which is expressed in Eq. (73) was eliminated by breaking each interval into three parts, as shown in Eqs. (76) and (77), respectively.

¹⁴Note: the subscripts a and b , attached to the index σ , indicate that a is a s' -root of $p_{\sigma_a,i}(s', z - v_h^{-1}|s - s'|) = 0$ and b is a s' -root of $p_{\sigma_b,i}(s', z - v_h^{-1}|s - s'|) = 0$, where σ_a may or may not equal σ_b .

The intervals $I_{i,k}^+$ are determined by the following algorithm:

1. Obtain the set of s' -roots $\{r_{\sigma,i,j}, j = 1, 2, \dots\}$ of $p_{\sigma,i}(s', z - v_h^{-1}|s - s'|) = 0$, for each σ .
2. Obtain the union $\{r_{i,j}\} = \cup_{\sigma}\{r_{\sigma,i,j}\}$ of all roots.
3. Sort the set $\{r_{i,j}\}$ into ascending order, and define the set of consecutive, open intervals $\{I_{i,j} = (r_{i,j}, r_{i,j+1})\}$.
4. Obtain the subset of intervals $\{I_{i,k}^+\} \subset \{I_{i,j}\}$, such that $p_{\sigma,i}(\mu_{i,j}, z - v_h^{-1}|s - \mu_{i,j}|) > 0$ for all σ , where $\mu_{i,j} = (r_{i,j} + r_{i,j+1})/2$ is the midpoint of the interval $I_{i,j}$.

C.1 Specifics for rhomboidal sources

For the rhomboidal source function, the set $\{p_{\sigma}\}$ has only one member; therefore, we drop the index σ . This single shape function is

$$p_i(s', z - v_h^{-1}|s - s'|) = L_x - \frac{L_x}{L_z} \left| z - \xi_i - \frac{1}{v_h} |s - s'| \right| - ||s'| - \beta_i| \quad (78)$$

and the corresponding charge profile is

$$g_i(s') = Q_{\min} + (Q_{\max} - Q_{\min}) (|s'| - \beta_i)^2, \quad (79)$$

where p_i and g_i are given by Eqs. (9) and (10), respectively, and the various parameters are described in Section (3.1).

Now, given Eqs. (78) and (79), the geometry-dependent details of the algorithm are as follows:

1. Obtain the set of roots $\{r_{i,j}\}$ of $p_i(s', z - v_h^{-1}|s - s'|) = 0$ by equating the RHS of Eq. (78) to zero and solving for s' . This entails the tedious process of unfolding pairs of nested absolute values - a process that yields 16 equations. These 16 equations are summarized as by

$$s'_{i,j} = \frac{T_{j,1}L_x + T_{j,2}\beta_i + T_{j,3}\lambda(z - \xi_i) + T_{j,4}\kappa\lambda s}{1 + T_{j,4}\kappa\lambda} \quad (80)$$

where $\lambda = L_x/L_z$, $\kappa = v_h^{-1}$ and $T_{j,\nu}$, $j = 1, 2, \dots, 16$, $\nu = 1, 2, 3, 4$ are elements of a 16×4 table of signs, with each of the 16 rows being a unique combination of four signs. However, only a subset of $\{s'_{i,j}\}$ actually satisfies $p_i(s', z - v_h^{-1}|s - s'|) = 0$. To determine this subset, we substituted each member of $\{s'_{i,j}\}$ into Eq. (78), to test whether the RHS is zero. The set of roots $\{r_{i,j}\}$ that we seek is the subset of the $\{s'_{i,j}\}$ whose members pass this test, i.e. $\{r_{i,j}\} \subset \{s'_{i,j} : p_i(s', z - v_h^{-1}|s - s'|) = 0\}$.

2. Because there is only one function p_i , the union over σ is just $\{r_{i,j}\}$.

After performing generic steps 3 and 4, we obtain the set of intervals $I_k^+ = (a_{i,k}, b_{i,k})$ for the rhomboidal source function. Also, from Eq. (79), we obtain

$$A_i(s') = Q_{\min}s' + (Q_{\max} - Q_{\min}) \left(\frac{(s')^3}{3} - \beta_i s' |s'| + \beta_i^2 s' \right) \quad (81)$$

which we used to compute $A_i(a_{i,k})$ and $A_i(b_{i,k})$ for all k , which we then substituted into Eqs. (75) and (77), respectively.

C.2 Specifics for rectangular sources

For the rectangular source function, the set $\{p_\sigma\}$ has two members are

$$p_{1,i}(s', z - v_h^{-1}|s - s'|) = L_z - \left| z - \xi_i - \frac{1}{v_h} |s - s'| \right| \quad (82)$$

and

$$p_{2,i}(s', z - v_h^{-1}|s - s'|) = L_x - ||s'| - \beta_i| \quad (83)$$

and the corresponding charge profile is

$$g_i(s') = Q_{\max}. \quad (84)$$

where $p_{1,i}$ and $p_{2,i}$ are given by the first two lines in Eq. (6), and where $g_i(s')$ is given by the third line in Eq. (6).

Now, given Eqs. (82) and (83), the geometry-dependent details of the algorithm are as follows:

1. Obtain the sets of roots $\{r_{\sigma,i,j}\}$ of $p_{\sigma,i}(s', z - v_h^{-1}|s - s'|) = 0$, for $\sigma = 1, 2$, by equating the RHS of both Eq. (82) and Eq. (83) to zero, and solving each equation for s' . This entails unfolding the nested absolute value in each equation, a process that yields four equations for each. It can be shown that these two sets of four equations are summarized by

$$s'_{1,i,j} = \frac{T_{j,1}L_z + T_{j,2}(z - \xi_i) + \kappa s}{\kappa} \quad (85)$$

and

$$s'_{2,i,j} = T_{j,1}L_x + T_{j,2}\beta_i \quad (86)$$

where $T_{j,\nu}$, $j = 1, 2, 3, 4$, $\nu = 1, 2$ are elements of a 4×2 table of signs, with each of the four rows being a unique combination of two signs. However, only a subset of each set $\{s_{\sigma,i,j}\}$ satisfies the corresponding equation $p_{\sigma,i}(s', z - v_h^{-1}|s - s'|) = 0$. To determine these subsets, we substituted each member of $\{s'_{1,i,j}\}$ and $\{s'_{2,i,j}\}$ into Eqs. (82) and (83), respectively, to test whether the RHS of each is zero. The two sets of roots $\{r_{1,i,j}\}$ and $\{r_{2,i,j}\}$ that we seek are the subsets of $\{s'_{1,i,j}\}$ and $\{s'_{2,i,j}\}$, whose members pass their respective tests, i.e. $\{r_{\sigma,i,j}\} \subset \{s'_{\sigma,i,j} : p_{\sigma,i}(s', z - v_h^{-1}|s - s'|) = 0\}$ for $\sigma = 1, 2$.

2. Because there are two function $p_{1,i}$ and $p_{2,i}$, we have $\{r_{i,j}\} = \cup_{\sigma} \{r_{\sigma,i,j}\} = \{r_{1,i,j}\} \cup \{r_{2,i,j}\}$.

After performing generic steps 3 and 4, we obtain the set of intervals $I_k^+ = (a_{\sigma_a i, k}, b_{\sigma_b i, k})$ for the rectangular source function. Note that, for some intervals, we may have $\sigma_a = \sigma_b$; that is, the bounds are the roots of the same function. Also, from Eq. (84), we obtain

$$A_i(s') = Q_{\max} s' \quad (87)$$

which we use to compute $A_i(a_{i,k})$ and $A_i(b_{i,k})$ for all k , which we then substitute into Eqs. (75) and (77), respectively.

D Partial Derivatives of the Shift Vector

In this appendix, we derive analytic expressions for the derivatives of the shift vector components. It is convenient to write two equations: one for the

three partial derivatives of N_z and one for the three partial derivatives of both N_x and N_y . We write these as follows:

$$\partial_u N_z(s, z) = -\frac{1}{4} v_h W \sum_{i=1}^4 \alpha_i \partial_u \mathcal{I}_{1,i}(s, z) \quad (88)$$

and

$$\partial_u N_v(s, z) = \frac{1}{4} W \frac{v}{|v|} \sum_{i=1}^4 \alpha_i \partial_u \mathcal{I}_{2,i}(s, z), \quad (89)$$

where $u \in \{x, y, z\}$, $v \in \{x, y\}$ and $\mathcal{I}_{1,i}$ and $\mathcal{I}_{2,i}$ are given by Eqs. (74) and (76), respectively.

D.1 Partial derivatives of the integrals $\mathcal{I}_{1,i}$ and $\mathcal{I}_{2,i}$

The first step in evaluating Eqs. (88) and (89) is to obtain expressions for $\partial_u \mathcal{I}_{1,i}$ and $\partial_u \mathcal{I}_{2,i}$. Expanding the derivatives in Eqs. (88) and (89), by substituting RHS of Eqs. (74) and (76), respectively, we obtain

$$\partial_u \mathcal{I}_{1,i}(s, z) = \sum_k \partial_u \int_{a_{\sigma_a, i, k}}^{b_{\sigma_b, i, k}} g_i(s') ds' \quad (90)$$

and

$$\partial_u \mathcal{I}_{2,i}(s, z) = \sum_k \begin{cases} \partial_u \int_{a_{\sigma_a, i, k}}^{b_{\sigma_b, i, k}} g_i(s') ds', & s > b_{\sigma_b, i, k} \\ -\partial_u \int_{a_{\sigma_a, i, k}}^{b_{\sigma_b, i, k}} g_i(s') ds', & s < a_{\sigma_a, i, k} \\ \partial_u \left(\int_{a_{\sigma_a, i, k}}^s g_i(s') ds' - \int_s^{b_{\sigma_b, i, k}} g_i(s') ds' \right), & a_{\sigma_a, i, k} < s < b_{\sigma_b, i, k} \end{cases} \quad (91)$$

Comparing Eq. (90) with Eq. (91), it can be observed that:

- The first line of the latter is identical to the former; that is, if $s > b_{\sigma_b, i, k}$, then $\partial_u \mathcal{I}_{2,i} = \partial_u \mathcal{I}_{1,i}$.
- The second line of the latter is the negative of the former; that is, if $s < a_{\sigma_a, i, k}$, then $\partial_u \mathcal{I}_{2,i} = -\partial_u \mathcal{I}_{1,i}$.

Using these facts, we may rewrite Eq. (91) as

$$\partial_u \mathcal{I}_{2,i}(s, z) = \sum_k \begin{cases} \partial_u \mathcal{I}_{1,i}(s, z), & s > b_{\sigma_b, i, k} \\ -\partial_u \mathcal{I}_{1,i}(s, z), & s < a_{\sigma_a, i, k} \\ \partial_u \left(\int_{a_{\sigma_a, i, k}}^s g_i(s') ds' - \int_s^{b_{\sigma_b, i, k}} g_i(s') ds' \right), & a_{\sigma_a, i, k} < s < b_{\sigma_b, i, k} \end{cases} \quad (92)$$

Thus, we can see that there are only two unique integrations to be evaluated. Recalling that the limits of integration $a_{\sigma_1, i, k}$ and $b_{\sigma_2, i, k}$ are the roots of equations $p_{\sigma, i}(s', z - v_h^{-1}|s - s'|) = 0$, and thus depend on the coordinates (s, z) , we use the standard result for differentiating a definite integral with variable limits. Doing this for Eq. (90) and the third line in Eq. (92), we obtain

$$\partial_u \mathcal{I}_{1,i}(s, z) = \sum_k (g_i(b_{\sigma_b, i, k}) \partial_u b_{\sigma_b, i, k} - g_i(a_{\sigma_a, i, k}) \partial_u a_{\sigma_a, i, k}) \quad (93)$$

and (after a bit of algebra)

$$\partial_u \mathcal{I}_{2,i}(s, z) = \sum_k (2g_i(s) \partial_u s - g_i(a_{\sigma_a, i, k}) \partial_u a_{\sigma_a, i, k} - g_i(b_{\sigma_b, i, k}) \partial_u b_{\sigma_b, i, k}) \quad (94)$$

respectively.

Substituting Eqs. (93) and (94) into (88) and (89), respectively, we obtain

$$\partial_u N_z(s, z) = -\frac{1}{4} v_h W \sum_{i=1}^4 \alpha_i \sum_k (g_i(b_{\sigma_b, i, k}) \partial_u b_{\sigma_b, i, k} - g_i(a_{\sigma_a, i, k}) \partial_u a_{\sigma_a, i, k}) \quad (95)$$

and

$$\partial_u N_v(s, z) = \frac{1}{4} W \frac{v}{|v|} \sum_{i=1}^4 \alpha_i \sum_k (2g_i(s) \partial_u s - g_i(a_{\sigma_a, i, k}) \partial_u a_{\sigma_a, i, k} - g_i(b_{\sigma_b, i, k}) \partial_u b_{\sigma_b, i, k}). \quad (96)$$

D.2 Partial derivatives of the roots a and b

As shown in Eqs. (93) and (94), we require the derivatives of the roots $a_{\sigma_1,i,k}$ and $b_{\sigma_2,i,k}$ with respect to the coordinates $u \in \{s, z\}$. Considering this, we define

$$P_{\sigma,i}(s, z) = p_{\sigma,i}(s', z - v_h^{-1}|s - s'|) \quad (97)$$

where for now s' is an arbitrary function of s and z . The total derivative of $P_{\sigma,i}$ is

$$\frac{dP_{\sigma,i}}{du} = \frac{\partial p_{\sigma,i}}{\partial s'} \frac{\partial s'}{\partial u} + \frac{\partial p_{\sigma,i}}{\partial u}. \quad (98)$$

Let $s'(s, z)$ be defined¹⁵ by $p_{\sigma,i}(s', z - v_h^{-1}|s - s'|) = 0$. Then, by using the definition in Eq. (97), $P_{\sigma,i}(s, z) = p_{\sigma,i}(s', z - v_h^{-1}|s - s'|) = 0$, so

$$\frac{\partial p_{\sigma,i}}{\partial s'} \frac{\partial s'}{\partial u} + \frac{\partial p_{\sigma,i}}{\partial u} = 0. \quad (99)$$

For clarity, we switch to index notation, wherein Eq. (99), can be written as

$$\partial_{s'} p_{\sigma,i} \partial_u s' + \partial_u p_{\sigma,i} = 0. \quad (100)$$

Then, solving Eq. 100 for $\partial_u s'$, we have

$$\partial_u s' = - \frac{\partial_u p_{\sigma,i}(s', z - v_h^{-1}|s - s'|)}{\partial_{s'} p_{\sigma,i}(s', z - v_h^{-1}|s - s'|)}. \quad (101)$$

Then, denoting roots $a_{\sigma_a,i,k}$ and $b_{\sigma_b,i,k}$ collectively by $r_{\sigma,i,k}$, we have

$$\partial_u r_{\sigma,i,k} = \partial_u s' |_{s'=r_{\sigma,i,k}} = - \frac{\partial_u p_{\sigma,i}(s', z - v_h^{-1}|s - s'|) |_{s'=r_{\sigma,i,k}}}{\partial_{s'} p_{\sigma,i}(s', z - v_h^{-1}|s - s'|) |_{s'=r_{\sigma,i,k}}} := -q_{\sigma,i,k}^u(r_{\sigma,i,k}), \quad (102)$$

¹⁵ s' is not uniquely defined, because there are multiple roots for each value of s and z . However, we will take one of those roots r_0 for a particular s_0 and z_0 and then define s' for points in the neighborhood of s_0 and z_0 to be the roots that are close to r_0 . This operation can be made mathematically rigorous, resulting in a differentiable function $s'(s, z)$. This procedure applies for each root.

where for convenience, we denote the quotient appearing in Eq. (102) by $q_{\sigma,i,k}^u$.

Now, recall that Eq. (102) represents three equations, due to $u \in \{x, y, z\}$. For clarity, we explicitly wrote these out (see Eqs. (103), (104) and (105), below). Additionally, for brevity, we suppress the arguments to the $p_{\sigma,i}$ (and bear in mind that the $p_{\sigma,i}$ are, in general, functions of s', s and z). For $u = z$, we have

$$\partial_z r_{\sigma,i,k} = \partial_z s' |_{s'=r_{\sigma,i,k}} = -\frac{\partial_z p_{\sigma,i} |_{s'=r_{\sigma,i,k}}}{\partial_{s'} p_{\sigma,i} |_{s'=r_{\sigma,i,k}}} := -q_{\sigma,i,k}^z(r_{\sigma,i,k}) \quad (103)$$

and, since $s = |x| + |y|$, for $u \in \{x, y\}$, we have

$$\partial_x r_{\sigma,i,k} = -\frac{\partial_s p_{\sigma,i} |_{s'=r_{\sigma,i,k}}}{\partial_{s'} p_{\sigma,i} |_{s'=r_{\sigma,i,k}}} \partial_x s := -q_{\sigma,i,k}^s(r_{\sigma,i,k}) \partial_x s = -\frac{x}{|x|} q_{\sigma,i,k}^s(r_{\sigma,i,k}) \quad (104)$$

and

$$\partial_y r_{\sigma,i,k} = -\frac{\partial_s p_{\sigma,i} |_{s'=r_{\sigma,i,k}}}{\partial_{s'} p_{\sigma,i} |_{s'=r_{\sigma,i,k}}} \partial_y s := -q_{\sigma,i,k}^s(r_{\sigma,i,k}) \partial_y s = -\frac{y}{|y|} q_{\sigma,i,k}^s(r_{\sigma,i,k}). \quad (105)$$

Next, substituting Eq. (102) into Eqs. (95) and (96), we obtain, respectively

$$\partial_u N_z(s, z) = -\frac{1}{4} v_h W \sum_{i=1}^4 \alpha_i \Omega_{1,i}^u \quad (106)$$

and

$$\partial_u N_v(s, z) = \frac{1}{4} W \frac{v}{|v|} \sum_{i=1}^4 \alpha_i \Omega_{2,i}^u. \quad (107)$$

where we have defined

$$\Omega_{1,i}^u = \sum_k (g_i(b_{\sigma_b,i,k}) q_{\sigma_b,i,k}^u(b_{\sigma,i,k}) - g_i(a_{\sigma_a,i,k}) q_{\sigma_a,i,k}^u(a_{\sigma,i,k})) \quad (108)$$

and

$$\Omega_{2,i}^u = \sum_k (2g_i(s)\partial_u s + g_i(a_{\sigma_a,i,k})q_{\sigma_a,i,k}^u(b_{\sigma,i,k}) + g_i(b_{\sigma_b,i,k})q_{\sigma_b,i,k}^u(b_{\sigma,i,k})) \quad (109)$$

Each of the Eqs. (106) and (107) represent the next three equations. That is, for $u = z, x, y$, we have

$$\partial_z N_z(s, z) = -\frac{1}{4}v_h W \sum_{i=1}^4 \alpha_i \Omega_{1,i}^z \quad (110)$$

$$\partial_x N_z(s, z) = -\frac{1}{4}v_h W \frac{x}{|x|} \sum_{i=1}^4 \alpha_i \Omega_{1,i}^x \quad (111)$$

$$\partial_y N_z(s, z) = -\frac{1}{4}v_h W \frac{y}{|y|} \sum_{i=1}^4 \alpha_i \Omega_{1,i}^y \quad (112)$$

and for $u \in \{x, y\}$, we have, respectively

$$\partial_x N_x(s, z) = \frac{1}{4}W \frac{x}{|x|} \frac{x}{|x|} \sum_{i=1}^4 \alpha_i \Omega_{2,i}^x, \quad v = x \quad (113)$$

$$\partial_x N_y(s, z) = \frac{1}{4}W \frac{x}{|x|} \frac{y}{|y|} \sum_{i=1}^4 \alpha_i \Omega_{2,i}^y, \quad v = y \quad (114)$$

$$\partial_y N_y(s, z) = \frac{1}{4}W \frac{y}{|y|} \frac{y}{|y|} \sum_{i=1}^4 \alpha_i \Omega_{2,i}^y, \quad v = y \quad (115)$$

and of course $\partial_y N_x = \partial_x N_y$, $\partial_z N_x = \partial_x N_z$ and $\partial_y N_z = \partial_z N_x$, accounting for all nine partial derivatives of the shift vector.

D.3 Partial derivatives of the shape functions

We now require expressions for the derivatives $\partial_z p_{\sigma,i}$ and $\partial_s p_{\sigma,i}$, which appear in the numerators of q^z and q^s , respectively, and $\partial_{s'} p_{\sigma,i}$, which appears in both denominators. These are provided for rhomboidal and rectangular shape functions in Sections D.3.1 and D.3.2, respectively.

D.3.1 Partial derivatives of the rhomboidal shape function

By taking the partial derivatives of Eq. 78 wrt z , s and s' , we obtain for any root r

$$\partial_z p_i(s', z - v_h^{-1}|s - s'|)|_{s'=r} = -\frac{L_x}{L_z} \frac{\eta(r)}{|\eta(r)|}, \quad \eta(r) \neq 0 \quad (116)$$

where

$$\eta(r) = z - \xi_i - \frac{1}{v_h}|s - r|, \quad (117)$$

$$\partial_s p_i(s', z - v_h^{-1}|s - s'|)|_{s'=r} = \frac{1}{v_h} \frac{L_x}{L_z} \frac{s - r}{|s - r|} \frac{\eta(r)}{|\eta(r)|}, \quad r \neq s, \eta(r) \neq 0 \quad (118)$$

and

$$\partial_{s'} p_i(s', z - v_h^{-1}|s - s'|)|_{s'=r} = -\frac{r}{|r|} \frac{|r| - \beta_i}{||r| - \beta_i|} - \frac{1}{v_h} \frac{L_x}{L_z} \frac{s - r}{|s - r|} \frac{\eta(r)}{|\eta(r)|}, \quad r \neq 0, |r| \neq \beta_i, \eta(r) \neq 0. \quad (119)$$

D.3.2 Partial derivatives of the rectangular shape functions

Here we have two shape functions, p_σ , $\sigma = 1, 2$, whose derivatives we treat separately.

Partial derivatives of p_1

By taking the partial derivatives of Eq. (82) wrt z , s and s' , we obtain for any root r

$$\partial_z p_{1,i}(s', z - v_h^{-1}|s - s'|)|_{s'=r} = -\frac{\eta(r)}{|\eta(r)|}, \quad \eta(r) \neq 0 \quad (120)$$

where $\eta(r)$ is given by Eq. (117),

$$\partial_s p_{1,i}(s', z - v_h^{-1}|s - s'|)|_{s'=r} = \frac{1}{v_h} \frac{s-r}{|s-r|} \frac{\eta(r)}{|\eta(r)|}, \quad r \neq s, \eta(r) \neq 0 \quad (121)$$

and

$$\partial_{s'} p_{1,i}(s', z - v_h^{-1}|s - s'|)|_{s'=r} = -\frac{1}{v_h} \frac{s-r}{|s-r|} \frac{\eta(r)}{|\eta(r)|}, \quad r \neq s, \eta(r) \neq 0 \quad (122)$$

Partial derivatives of p_2

By taking the partial derivatives of Eq. (83) wrt z , s and s' , we obtain

$$\partial_z p_{2,i}(s', z - v_h^{-1}|s - s'|)|_{s'=r} = 0, \quad (123)$$

$$\partial_s p_{2,i}(s', z - v_h^{-1}|s - s'|)|_{s'=r} = 0 \quad (124)$$

and

$$\partial_{s'} p_{2,i}(s', z - v_h^{-1}|s - s'|)|_{s'=r} = -\frac{r}{|r|} \frac{|r| - \beta_i}{||r| - \beta_i|}, \quad r \neq 0, |r| \neq \beta_i. \quad (125)$$

D.4 Extensions

From the above equations, we see that the partial derivatives of the shift vector are undefined under various circumstances. We refer to the domains of undefinition as ‘‘singular regions.’’ It is clear that our theory needs to be modified slightly so that these quantities are no longer undefined. However, different modifications generally lead to different values of those partial derivatives. Various principles can be invoked to limit the ambiguities. Most importantly, we would like physically measurable quantities to be insensitive to modification. For example, we require that integrals of the energy density are independent of these modifications. This is easily achieved when the singular regions lie along a set of measure 0 (in 3D). In that case, we can extend our functions such that, along these regions, the assigned values are finite.

Any finite assignment results in identical integrated values. We believe that with these finite assignments, other physically measurable quantities will also be independent of the values of their values. In the tables that follow, we indicate the particular circumstances and the equations that indicate those circumstances, for which each of the above-mentioned partial derivatives are undefined. We then go on to state the finite values we have used to extend our functions into singular regions.

Circumstances under which partials of the shift vector are undefined:

Partial of shift vector	Eq.	Circumstances
$\partial_z N_z$ undefined	(110)	q^z undefined
$\partial_x N_z$ undefined	(111)	$x = 0$ or q^s undefined
$\partial_y N_z$ undefined	(112)	$y = 0$ or q^s undefined
$\partial_x N_x$ undefined	(113)	$x = 0$ or q^s undefined
$\partial_y N_y$ undefined	(115)	$y = 0$ or q^s undefined
$\partial_x N_y$ undefined	(114)	$x = 0, y = 0$ or q^s undefined

Circumstances under which quotients q^z and q^s are undefined:

Quotient	Eq.	Circumstances
q^z undefined	(102)	$\partial_z p_{\sigma,i}$ or $\partial_{s'} p_{\sigma,i}$ undefined
q^s undefined	(104)	$\partial_s p_{\sigma,i}$ or $\partial_{s'} p_{\sigma,i}$ undefined

Circumstances under which partials of the rhomboidal shape function is undefined:

Partial of shape func	Eq.	Circumstances
$\partial_z p_i$ undefined	(116)	$\eta(r) = 0$
$\partial_s p_i$ undefined	(118)	$r = s$ or $\eta(r) = 0$
$\partial_{s'} p_i$ undefined	(119)	$r = 0, r = \beta_i, r = s$ or $\eta(r) = 0$

Circumstances under which partials of the rectangular shape p_1 are undefined:

Partial of shape func	Eq.	Circumstances
$\partial_z p_{1,i}$ undefined	(120)	$\eta(r) = 0$
$\partial_s p_{1,i}$ undefined	(121)	$r = s$ or $\eta(r) = 0$
$\partial_{s'} p_{1,i}$ undefined	(122)	$r = s$ or $\eta(r) = 0$

Circumstances under which partials of the rectangular shape p_2 are undefined:

Partial of shape func	Eq.	Circumstances
$\partial_z p_{2,i}$ undefined	(120)	None
$\partial_s p_{2,i}$ undefined	(121)	None
$\partial_{s'} p_{2,i}$ undefined	(122)	$r = 0$ or $ r = \beta_i$

Ultimately, all the above circumstances occur at points where expressions for the partials of the shift vector or of the shape function contain a factor of the form $w/|w|$, which is undefined at $w = 0$. At such points, reasonable values are assigned, thereby extending (or completing) the expressions for the derivatives at the points in question.

For mixed derivatives of the shift vector, that is, $\partial_u N_v$, $u \neq v$, there are overall factors $u/|u|$, $u \in \{x, y\}$. A reasonable extension for these points consists of substituting the signum function $\text{sgn}(u)$ for all ratios $u/|u|$, with the usual convention that $\text{sgn}(0) = 0$. Because $\text{sgn}(u)$ is equivalent to the original ratio everywhere except at $u = 0$, we merely substitute zero at $u = 0$. On the other hand, for pure derivatives of the shift vector, i.e. $\partial_u N_u$, the substitution produces the factor $\text{sgn}^2(u)$. As this has a value of 1 for all $u \neq 0$, it is reasonable to set $\text{sgn}^2(u) = 1$ at $u = 0$.

For derivatives of the shape function, we assign different extensions depending on whether we are dealing with the rhomboidal or rectangular case, as discussed in Sections D.4.1 and D.4.2, respectively.

D.4.1 Extensions for the rhomboidal case

Here, all the undefined points result from expressions of the form $w/|w|$. Following the same reasoning as above, all extensions for the rhomboidal case involve substituting the signum function $\text{sgn}(w)$ for all ratios $w/|w|$. There is one possible objection to this choice, which we will now lay to rest. Note that $\partial_{s'} p$ appears in the denominator of the quotients, as shown in

Eq. (102), and for rhomboidal case, $\partial_{s'}p$ is given by Eq. (119). According to the latter, two terms depend on the ratios of the form $w/|w|$. Thus, if one such ratio in each term is set to zero, then the quotients are undefined. Specifically, if either $r = 0$ or $|r| = \beta_i$, while at the same point either $r = s$ or $\eta(r) = 0$, the quotients are undefined. Fortunately, none of these conditions were observed.

D.4.2 Extensions for the rectangular case

We *cannot* universally use the same approach here as for the rhomboidal case (i.e. substituting $\text{sgn}(w)$ for $w/|w|$), because in the rectangular case $\partial_{s'}p$ consists of only one term, according to Eqs. (122) and (125). Thus, the quotient in Eq. (102) is undefined if either $r = s$ or $\eta(r) = 0$ and the quotient in Eq. (104) is undefined if either $r = 0$ or $|r| = \beta_i$. We can avoid this issue by working at the level of the quotients, rather than the individual derivatives.

Extensions for shape function p_1

We note from Eqs. (121) and (122) that $\partial_{s'}p_1 = -\partial_s p_1$ and thus

$$q^s(p_1) = \frac{\partial_s p_1}{\partial_{s'} p_1} = \frac{\partial_s p_1}{-\partial_s p_1} = -1 \quad r \neq s, \eta(r) \neq 0. \quad (126)$$

The reasonable extension here is to ignore the restrictions, i.e. always set

$$q^s(p_1) = -1 \quad (127)$$

Next, we note from Eqs. (122) and (120) that

$$\partial_{s'} p_1 = \frac{1}{v_h} \frac{s-r}{|s-r'|} \partial_z p_1 \quad (128)$$

and thus

$$q^z(p_1) = \frac{\partial_z p_1}{\partial_{s'} p_1} = \frac{\partial_z p_1}{\frac{1}{v_h} \frac{s-r}{|s-r'|} \partial_z p_1} = v_h \left(\frac{s-r}{|s-r'|} \right)^{-1} = v_h \frac{s-r}{|s-r|}, \quad r \neq s. \quad (129)$$

Then, by reasoning analogous to Section D.4.1, we have

$$q^z(p_1) = v_h \text{sgn}(s - r). \quad (130)$$

Extensions for shape function p_2 We note from Eqs. (125) and (124) that

$$q^s(p_2) = \frac{\partial_s p_2}{\partial_{s'} p_2} = \frac{0}{\partial_{s'} p_{i,2}} = 0, \quad r \neq 0, |r| \neq \beta_i. \quad (131)$$

The reasonable extension here is to ignore the restrictions, i.e. always set

$$q^s(p_2) = 0. \quad (132)$$

Next, we note from Eqs. (125) and (123) that

$$q^z(p_2) = \frac{\partial_z p_{i,2}}{\partial_{s'} p_{i,2}} = \frac{0}{\partial_{s'} p_{i,2}} = 0, \quad r \neq 0, |r| \neq \beta_i. \quad (133)$$

Once again, the reasonable extension is to ignore the restrictions, i.e. always set

$$q^z(p_2) = 0. \quad (134)$$

D.5 Algorithmic Differentiation

Depending on the complexity of the expressions for the shift vector components, deriving expressions for the corresponding partial derivatives can be extremely time consuming, and may lead to unwieldy expressions that are difficult to check. This is the case for the partial derivatives of N_y in Lentz's original equations. However, these partial derivatives are required to obtain the image shown in Fig. 4. (Recall that partial derivatives of the shift vector are required to calculate the Eulerian energy density.) Therefore, rather than deriving analytic expressions using symbolic differentiation, *Algorithmic Differentiation* (AD) was used to obtain the required partial derivatives.

D.5.1 General principles of algorithmic differentiation

AD differs from symbolic differentiation in several ways.

- Symbolic differentiation: You manipulate formulas to obtain a new symbolic expression for $f'(x)$. Once you have that expression, you can plug in any x . For example, from $f(x) = \sin(x) + x^2$ you derive $f'(x) = \cos(x) + 2x$, then you evaluate at $x = 2$.
- Algorithmic Differentiation (AD): You never build a closed-form expression for $f'(x)$. Instead:
 1. You record (or trace) the sequence of elementary operations that compute $f(x)$.
 2. You propagate derivatives numerically through that sequence using the chain rule.
 3. The chosen point x is supplied before or at the start of the derivative sweep; therefore, the chain rule is applied to actual numeric values, not symbolic placeholders. Thus, AD produces a numeric derivative at that point, not a symbolic formula for $f'(x)$.

Standard symbolic differentiation can lead to a much higher computational complexity than algorithmic differentiation. This is illustrated in the following example. Consider a recursively nested function

$$f_n(x) = \sin(\sin(\sin(\cdots \sin(x) \cdots))),$$

where \sin is applied n times.

- Symbolic differentiation: By the chain rule,

$$f'_n(x) = \cos(f_{n-1}(x)) \cdot f'_{n-1}(x).$$

If expanded fully:

$$f'_n(x) = \cos(\sin(\sin(\cdots \sin(x)))) \cdot \cos(\sin(\sin(\cdots \sin(x)))) \cdots \cos(x),$$

with n nested cosine factors. For $n = 3$:

$$\begin{aligned} f_3(x) &= \sin(\sin(\sin(x))), \\ f'_3(x) &= \cos(\sin(\sin(x))) \cdot \cos(\sin(x)) \cdot \cos(x). \end{aligned}$$

For large n , the expression becomes enormous: it involves $O(n^2)$ trigonometric operations.

- Algorithmic differentiation: At a chosen point x , AD computes numerically, the following:

$$\begin{aligned} v_0 &= x, & d_0 &= 1, \\ v_k &= \sin(v_{k-1}), \\ d_k &= \cos(v_{k-1}) \cdot d_{k-1}, & k &= 1, \dots, n. \end{aligned}$$

At the end, $f_n(x) = v_n$ and $f'_n(x) = d_n$. This requires $O(n)$ operations.

It should be noted that the above symbolic differentiation can be accomplished more efficiently by re-using sub-expressions. In more general cases, this approach is known as structured symbolic differentiation. It can be a somewhat difficult and error-prone task to setup and code an ad hoc structured symbolic differentiation algorithm. AD is just a restricted, disciplined form of structured symbolic differentiation, for which prepackaged tools have been created.

Importantly, AD is not equivalent to numerical methods such as finite-difference algorithms. If the function to be differentiated is smooth at a given point, the result is highly accurate. It does not suffer from round-off error and truncation errors, unlike the finite differences method. In the latter, there is a trade-off between these two types of error, such that the best one can hope for is nearly single-precision accuracy in double-precision calculations. However, AD is normally accurate to the full precision of the machine.

For the modified version of Lentz's warp drive, we ran a comparison of the partial derivatives of the shift vector, as generated by AD and by the analytic expressions, at all grid points, and found that the results are in complete agreement.¹⁶ This has given us confidence in applying AD to calculate these partial derivatives for Lentz's original warp drive.

¹⁶This holds, except where extensions have not been applied in the AD case (e.g. the planes $x = 0$ and $y = 0$).

D.5.2 AD for N_y in Lentz's original warp drive

Of course, one cannot expect AD to produce a meaningful result¹⁷ for a particular partial derivative, if that derivative or the function itself is undefined at the given point. As we have seen for the modified Lentz geometry discussed in Section D.4, the shift vector has such points, which should be avoided when using AD.

As a practical matter, calculations of the shift vector components, their derivatives and the Eulerian energy density are performed at a finite number of locations, which are at points on a regularly-spaced grid. The grid is set up such that the x -, y -, and z -axes coincide with grid lines, and the spacing of the grid is such that all centerlines of the rhomboids coincide with grid lines. As discussed in Section 3.3, we avoided possible ambiguities at $y = 0$ by taking the slices at $y = 10^{-6}$. This was implemented by shifting the entire grid by 10^{-6} , along the y direction.

E Estimating Total Energy

As discussed in section 5.2, the energy density at a point in space is the sum of what we call the U and the T terms.

Based on the assumption that the energy density at a grid point is approximately constant over the grid cell containing that point, the total contribution from the U term is estimated by adding the energy density at all grid points and multiplying by the cell volume, i.e.

$$U_{tot} \approx \Delta^3 \sum_i \sum_j \sum_k E_{i,j,k} \quad (135)$$

where Δ denotes the fixed grid spacing.

The total contribution from the T term is estimated by adding up the contributions at all grid points in the planes $x = 0$ and $y = 0$. (The T term is zero at all other grid points). We now derive the approximate expression for the contribution of the T term to the total energy. Based on the definition

¹⁷Packaged AD applications may employ extensions similar to ours, but that remains to be investigated.

of T , the integral over all space of T is given by

$$\begin{aligned}
T_{tot} &= 2 \int_{z=-\infty}^{\infty} \int_{y=-\infty}^{\infty} \int_{x=-\infty}^{\infty} \delta(x) A(x, y, z) dx dy dz \\
&+ 2 \int_{z=-\infty}^{\infty} \int_{y=-\infty}^{\infty} \int_{x=-\infty}^{\infty} \delta(y) A(x, y, z) dx dy dz \\
&+ 4 \int_{z=-\infty}^{\infty} \int_{y=-\infty}^{\infty} \int_{x=-\infty}^{\infty} \delta(x) \delta(y) B(x, y, z) dx dy dz \quad (136)
\end{aligned}$$

where

$$A = \partial_s \phi (\partial_s^2 \phi + \partial_z N_z) \quad (137)$$

and

$$B = (\partial_s \phi)^2. \quad (138)$$

From the distributional properties of the deltas, we can immediately rewrite Eq. (136) as

$$T_{tot} = 2 \int_{z=-\infty}^{\infty} \int_{y=-\infty}^{\infty} A(0, y, z) dy dz + 2 \int_{z=-\infty}^{\infty} \int_{x=-\infty}^{\infty} A(x, 0, z) dx dz + 4 \int_{z=-\infty}^{\infty} B(0, 0, z) dz \quad (139)$$

and using the same reasoning regarding the grid as before, we can estimate T_{tot} via

$$T_{tot} \approx 2\Delta^2 \sum_i \sum_j A(0, y_j, z_i) + 2\Delta^2 \sum_i \sum_k A(x_k, 0, z_i) + 4\Delta \sum_i B(0, 0, z_i). \quad (140)$$

It is expected that the estimates of U_{tot} and T_{tot} improve as Δ shrinks.

F A counterexample to the shift-derivative inequality

Our counter-example will use the function

$$\rho(\alpha, s') = (1 - |s'|)e^{-\alpha^2}. \quad (141)$$

Set $\alpha = (z - |s - s'|)$. Then $\partial_z \rho(\alpha, s') = -2(z - |s - s'|)\rho(\alpha, s')$. Set $z = 0$ and $s > 0$. Then Eqs. (26) become,

$$\begin{aligned} |\partial_z^2 \phi| &= \frac{1}{2} \left| \int_{-\infty}^{\infty} ds' (1 - |s'|) |s - s'| e^{-(s-s')^2} \right| \\ |\partial_z \partial_s \phi| &= \frac{1}{2} \left| \int_{-\infty}^{\infty} ds' \operatorname{sgn}(s - s') (1 - |s'|) |s - s'| e^{-(s-s')^2} \right| \end{aligned} \quad (142)$$

These integrals can be computed analytically by first dividing them into three regions. Define I_1 , I_2 and I_3 as

$$\begin{aligned} I_1 &= \int_s^{\infty} ds' (1 - s')(s' - s) e^{-(s-s')^2} \\ I_2 &= \int_0^s ds' (1 - s')(s - s') e^{-(s'-s)^2} \\ I_3 &= \int_{-\infty}^0 ds' (1 + s')(s - s') e^{-(s'-s)^2} \end{aligned} \quad (143)$$

We then compute the integrals and from Eq. (144) we have

$$\begin{aligned} |\partial_z^2 \phi| &= \frac{1}{2} |I_1 + I_2 + I_3| = \frac{1}{2} \left| 1 - s - \frac{1}{2} \Gamma\left(\frac{1}{2}, s^2\right) \right|, \\ |\partial_z \partial_s \phi| &= \frac{1}{2} |-I_1 + I_2 + I_3| = \frac{1}{2} \left| \frac{\sqrt{\pi}}{2} - \frac{1}{2} \Gamma\left(\frac{1}{2}, s^2\right) \right|, \end{aligned} \quad (144)$$

where the Γ 's are incomplete gamma functions. For example, assume $s = 1$. Then $|\partial_z^2 \phi|(1, 0, 0) = 0.07$ and $|\partial_z \partial_s \phi|(1, 0, 0) = 0.4$. Therefore $|\partial_z^2 \phi|(1, 0, 0) < |\partial_z \partial_s \phi|(1, 0, 0)$, thereby contradicting the shift-derivative inequality.¹⁸

¹⁸If we change s and s' to x and x' then the shift-derivative inequality becomes equivalent to Lentz's inequality in Ref. [31].

G Graphics

Two types of graphical representations of the quantities of interest are used in the figures shown in this paper:

- A *Planar cross-section* provides an excellent depiction of the spatial structure of a quantity, but only a vague sense of the numerical values of this quantity, as it varies over the plane. This is because the numerical values are conveyed using color intensity, for which the human eye is not well-adapted to discern differences. (More about this below.)
- A *Profile* provides an excellent depiction of the numerical values of a quantity, as it varies along a specific line, but being confined to that specific line, it does not convey much information about spatial structure.

The two types of figure are discussed in Appendices G.1 and G.2. In both cases, graphical representations are created from quantities that computed at all points on a dense, 3-dimensional grid. However, the grid is constructed to be compatible with the image format used for planar cross-sections. The grid structure is also discussed in Appendix G.1.

G.1 Planar cross-sections

The 3-dimensional grid on which quantities are computed has the following properties:

- It covers a finite volume of a space-like hypersurface, which is represented Cartesian coordinate system.
- This volume has the shape of a cube centered a the origin of the Cartesian coordinate system.
- The cube is oriented such that each Cartesian axis intersects the center point of a pair of opposite faces.
- Grid points are equally spaced along the Cartesian axes, and along all lines parallel to them, each of which passes through one of the former.

We define a planar cross-section as a 2-dimensional slice of the grid, which is orthogonal to one of the Cartesian axes (and thus parallel to the plane defined by the other two axes) and centered at one of the grid points on the orthogonal axis.

However, the appropriate resolution of the grid remains to be determined. Planar cross-sections are displayed in a square image, consisting of 301×301 pixels. An odd number of pixels is chosen so that the center of the cross-section can be exactly centered in the image (with 150 pixels on either side of that origin in each dimension). The total number of pixels (301) across the image was chosen to be of sufficient density to create the illusion of continuity across the image, despite the fact that the data are generated at discrete locations. Thus, to achieve maximum resolution, the 3-dimensional grid must be $301 \times 301 \times 301$ points, so that a planar cross-section of the grid may be put into 1-to-1 correspondence with the pixels in the image. At this resolution there are $301^2 = 90,601$ points on each planar cross-section and $301^3 = 27,270,901$ points on the entire grid.

For each pixel in the image, we must supply a color and intensity that, together, represents a numerical value of the quantity. This graphical representation is implemented using OpenGL, which requires that the real values of the color intensity be in the range $[0, 1]$, where the intensity scale is linear. That is, an intensity of 1 corresponds to maximum brightness and an intensity of 0.5 is exactly half as bright, 0.25 a quarter as bright, etc., with 0 intensity being black. The linearity of intensity exacerbates the problem mentioned above (that the human eye is not well-adapted to discern differences in intensity). This is because the human eye does not perceive brightness linearly. In particular, dark regions with intensities as high as 0.15 are perceived as black, that is, indistinguishable from zero intensity.

G.1.1 γ -correction

A well-established remedy for the problem described in the preceding paragraph is γ -correction, in which intensity values are modified according to the formula $V_{\text{out}} = V_{\text{in}}^\gamma$, where it is required that $V_{\text{in}} \geq 0$ and $\gamma \in [0, 1]$. Thus, $\gamma = 1$ implies no γ -correction and the smaller the γ the greater the correction. Note that, for $V_{\text{in}} \in [0, 1]$ as required by OpenGL, if some non-trivial actual γ -correction is applied, that is, $\gamma < 1$, it will have no effect at the top of the scale, that is, $1^\gamma = 1$, and has increasing impact as $V_{\text{in}} \rightarrow 0$, shifting values towards higher intensity, such that the smaller the value V_{in} ,

the greater the shift. For example, suppose $\gamma = 0.5$: if $V_{\text{in}} = 0.5$, then $V_{\text{in}}^\gamma = 0.7 = 1.4V_{\text{in}}$, whereas if $V_{\text{in}} = 0.25$, then $V_{\text{in}}^\gamma = 0.5 = 2V_{\text{in}}$, and if $V_{\text{in}} = 0.125$, then $V_{\text{in}}^\gamma = 0.35 = 2.8V_{\text{in}}$.

Note that too much γ -correction, that is, very small values of γ , is counter-productive, as it tends to make all points equally bright. Thus, although no details are hidden, there appears to be little or no variability in the intensity.

G.1.2 Algorithm for the conversion of computed values to color intensities

Based on the preceding discussion, a computed value V_c of a physical quantity is processed as follows:

1. V_c is normalized by the largest absolute value, among all computed values of that quantity, i.e. $V_n = V_c/|V_c|_{\text{max}}$.
2. The desired γ -correction is applied, that is, $V_{n,\gamma} = |V_n|^\gamma$.
3. If $V_n < 0$, then $V_{n,\gamma}$ is passed to OpenGL, as the red intensity; otherwise, it is passed to OpenGL as the green intensity.

Owing to the normalization step, the final graphical representation of a planar cross-section cannot convey any information about the true range of values. Therefore, each planar cross-section is accompanied by a legend (on the right) that shows the true range of values.

G.2 Profiles

A profile can be obtained for any line on the planar cross-section for a particular quantity. Thus, lines parallel to either edge of the cross-section, that is, parallel one Cartesian axis, will have, at most, 301 points. (These are the only types of profiles used in this study.) This is sufficient to provide a continuous appearance to the resultant graphs, at the fixed, chosen size for those graphs. Thus, the graph shows the actual numerical values (not the normalized values) of a particular, computed quantity, as it varies along the chosen line, with the computed values as the ordinates and values of one Cartesian coordinate as the abscissae. The graphs were produced using GNUplot.

H Superluminal travel

Alcubierre [1] introduced warp drives as geometries which permit an observer to move in free fall at superluminal speeds relative to asymptotic time, and whose proper time is not dilated relative to the asymptotic time. In this appendix, we demonstrate that these properties can be obtained from the geometry generated by a hyperbolic potential (HP). In particular, we show that any HP with velocity \mathbf{v} can be scaled so that it permits an observer to move in free fall at velocity \mathbf{v} and without time dilation. The analysis closely follows that of Shoshany [30].

Recall the metric given by Eq. (2)

$$\begin{aligned} ds^2 &= -(1 - N^i N_i) dt^2 - 2N_i dx^i dt + \sum_{i=1}^3 dx^{i2} \\ &= -dt^2 + \sum_i (N_i dt - dx^i)^2. \end{aligned} \tag{145}$$

Note that if τ is the proper time, and if an object follows the trajectory $(t(\tau), \mathbf{x}(\tau))$ such that $\mathbf{x}(\tau) = \mathbf{x}_0 + \mathbf{N}t(\tau)$, then $(N_i dt - dx^i) = 0$ so that $ds^2 = -dt^2$. However, for a timelike path, the proper time is just $\sqrt{-ds^2}$, so $dt = d\tau$. Thus, such an object does not exhibit time dilation.

Is such an object in free fall? In other words, is the object's trajectory a geodesic? A geodesic is an extremal of the proper time

$$\begin{aligned} \tau &= \int \mathcal{L} d\lambda \\ &= \int \sqrt{-g_{\mu\nu} \dot{x}^\mu \dot{x}^\nu} d\lambda, \end{aligned} \tag{146}$$

where \dot{x}^α denotes $\frac{dx^\alpha}{d\lambda}$. The integral can be shown to be independent of the parameter λ so we can take $\lambda = \tau$. For our geometry,

$$ds^2 = g_{\mu\nu} dx^\mu dx^\nu, \tag{147}$$

and the values of $g_{\mu\nu}$ are given by

$$\begin{aligned} g_{00} &= -1 + N_i N^i \\ g_{0i} &= -N_i \\ g_{ij} &= \delta_{ij}. \end{aligned} \tag{148}$$

To find extrema, we solve the Euler-Lagrange equation

$$\frac{d}{d\tau} \left(\frac{\partial \mathcal{L}}{\partial \dot{x}^\alpha} \right) - \frac{\partial \mathcal{L}}{\partial x^\alpha} = 0. \quad (149)$$

We have

$$\frac{\partial \mathcal{L}}{\partial \dot{x}^\alpha} = \frac{-g_{\alpha\mu} \dot{x}^\mu}{\sqrt{-g_{\mu\nu} \dot{x}^\mu \dot{x}^\nu}} \quad (150)$$

and

$$\frac{\partial \mathcal{L}}{\partial x^\alpha} = \frac{-\partial_\alpha g_{\mu\nu} \dot{x}^\mu \dot{x}^\nu}{2\sqrt{-g_{\mu\nu} \dot{x}^\mu \dot{x}^\nu}} \quad (151)$$

Consider an ansatz for the solution of these E-L equations.

$$(\dot{t}, \dot{\mathbf{x}}) = (1, \mathbf{N}). \quad (152)$$

Note that if observers have a 4-velocity $(1, \mathbf{N})$, they are Eulerian observers. Start with the time component.

$$\frac{d}{d\tau} \frac{((1 - N^2) + N^2)}{\sqrt{((1 - N^2) + 2N^2 - N^2)}} - \frac{-2\partial_\alpha N_i N^i + 2\partial_\alpha N_i N^i}{2\sqrt{((1 - N^2) + 2N^2 - N^2)}} = \frac{d}{d\tau}(1) - 0 = 0. \quad (153)$$

The spacial-components are similar.

$$\frac{d}{d\tau} \frac{(N_i - N_i)}{2\sqrt{((1 - N^2) + 2N^2 - N^2)}} - \frac{-(2N^j \partial_i N_j - 2N^j \partial_i N_j)}{2\sqrt{((1 - N^2) + 2N^2 - N^2)}} = 0. \quad (154)$$

Therefore, we established that our ansatz is a solution to the E-L equations. From this it follows that

$$\frac{d\mathbf{x}}{dt} = \mathbf{N}. \quad (155)$$

In summary, we have shown that if an object travels with a velocity \mathbf{N} , then it is in free-fall, and its proper time is t ; that is, it experiences no time dilation. Interestingly, we have nowhere referred to the velocity of the warp drive, which we'll call \mathbf{v}' . If the free-falling object's velocity \mathbf{N} is different from \mathbf{v}' , then even if it starts off in the center of the warp drive (however we define that), it will move away from the center and eventually towards regions of the warp drive with ever smaller values of \mathbf{N} . If we want to arrange a situation where the freely-falling object remains in the center of the warp drive – and thus continues to experience the same value of \mathbf{N} and therefore

the absence of time dilation – then we must have $\mathbf{v}' = \mathbf{N}$. For the HP's, we can control the value of N by modifying various parameters, so we can set up a warp drive with a velocity \mathbf{v}' and, at its central point, $\mathbf{v}' = \mathbf{N}$. An object moving freely in the center of the warp drive will continue to stay in the center of the drive, and will experience no time dilation. If the region around the center of the warp drive has a level shift vector (i.e. \mathbf{N} is constant in that region), then an object moving (by non-gravitational forces) within that central region will continue to stay in that region.

I The y -dependence of the original and the modified Lentz warp drives

Lentz's original warp drive is based on the potential ϕ_L , which we observed to be asymmetric in the exchange of x and y . The source function and shift vectors for $y = 0$ should be the same (up to a certain sign) for ϕ_L (Eq. (6)) geometry and ϕ_{rh} (Eq. (29)). However, the two geometries differ, away from $y = 0$. The Eulerian energy density at $y = 0$ is dependent on the y -component of the shift vector as well as the y -dependence of all components of the shift vector. Therefore the Eulerian energy density is different for the ϕ_L geometry than for the ϕ_{rh} geometry.

Here we show N_y^{rh} and N_y^L . Notice that these exhibit discontinuities around the y -axis.

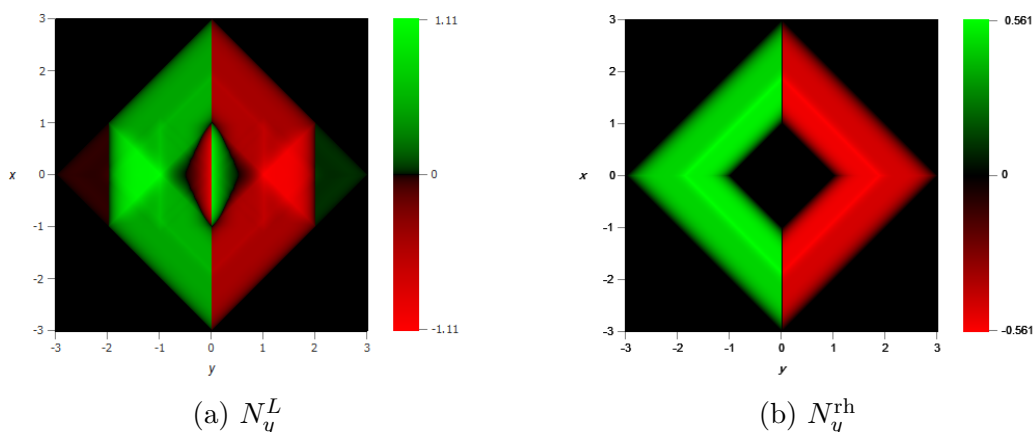


Figure 18: The shift vector components evaluated on the slice $z = 0$. The graphics gamma correction value (see Appendix G.1.1) is set to $\gamma = 0.5$.

We show further detail on the N_y^{rh} discontinuity, in Fig. 19 where we plot the profile $N_y^{\text{rh}}(x, y, z)$ at a single (x, z) value. The figure also shows the antisymmetry of N_y^{rh} around $y = 0$.

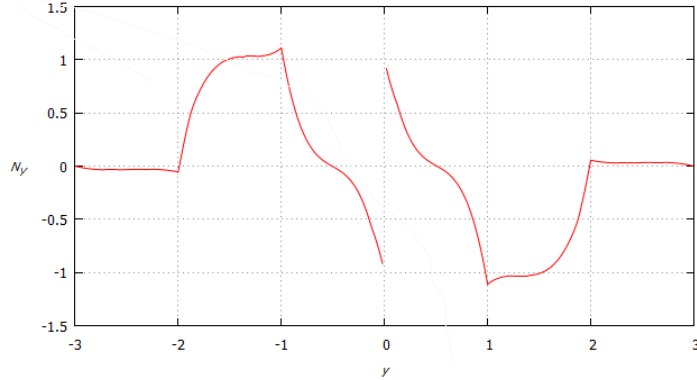


Figure 19: The profile N_y^{L} at fixed $(z, x) = (0, 0)$.

J Boundedness of the Shift Vector Domain

For our proof of finiteness, we repeat the conditions described in Section 4.3:

- The linear-cancellation condition

$$\int_{-\infty}^{\infty} ds' \rho(s', \alpha \pm s') = 0 \quad (156)$$

for any constant α .

- The source-domain boundedness condition

$$\begin{aligned} \rho \text{ has a bounded domain such that } \rho(s, z) = 0 \\ \text{if } |z| > B \text{ or } |s| > B \end{aligned} \quad (157)$$

for some B .

Our proof in Appendix J.1 will also depend on the definition $s(x, y) = |x| + |y|$, from which we can conclude that $s > 0$ and from which we can also conclude (which we use at the end of our proof) that if $|x| > B$ or $|y| > B$, then $s > B$. We also show in Appendix J.2 that if $s(x, y) = x + y$, no such proof is possible. Thus, for these definitions of s , the domain of the shift vector components is not bounded; therefore, the energy is not finite.

J.1 Boundedness of the shift vector domain when $s(x, y) = |x| + |y|$

From our expression Eq. (29) for the potential and the definition of the shift-vector, we obtain the shift components (again setting $v_h = 1$)

$$\begin{aligned} N_x &= \partial_x \phi = \frac{1}{4} \text{sgn}(x) \int_{-B}^B ds' \text{sgn}(s - s') \rho(s', z - |s - s'|), \\ N_y &= \partial_y \phi = \frac{1}{4} \text{sgn}(y) \int_{-B}^B ds' \text{sgn}(s - s') \rho(s', z - |s - s'|), \\ N_z &= \partial_z \phi = -\frac{1}{4} \int_{-B}^B ds' \rho(s', z - |s - s'|), \end{aligned} \quad (158)$$

where we use the bounds $\pm B$ as the limits of integration (rather than $\pm\infty$).

To show the boundedness of the N_i domain, it suffices to find Z_b, X_b, Y_b so that $N_i(x, y, z) = 0$ unless $|z| \leq Z_b$, and $|x| \leq X_b$ and $|y| \leq Y_b$.

- Large z .
 - First, consider $z \geq 4B$ and $s > 2B$. Examine the integrand(s). We know that $s' \leq B$ so $|s - s'| = s - s'$ and $z - |s - s'| = z - s + s'$. Also $\text{sgn}(s - s') = 1$. The N_i are then proportional to $\int_{-\infty}^{\infty} ds' \rho(s', (z - s) + s')$. We see this is of the form of the linear-cancellation condition and therefore $N_i = 0$.
 - Next, consider $z \geq 4B$ and $0 \leq s \leq 2B$. Since $-B \leq s' \leq B$, we can derive $-B \leq (s - s') \leq 3B$ and therefore $|s - s'| \leq 3B$. From this, we get $z - |s - s'| \geq 4B - 3B = B$. Therefore, in the integrands we have $\rho(s', z - |s - s'|) = 0$ since the second argument is greater than B . Hence, again, $N_i = 0$.
- Large $-z$. Consider $z \leq -3B$. But then $z - |s - s'| < -3B$, so the second argument of ρ (in the integrand) is less than $-B$ so $\rho(s', z - |s - s'|) = 0$ for all s' and therefore $N_i = 0$.
- Large s . Consider $s \geq B$. Then, since $s' \leq B$, we have $|s - s'| = s - s'$ and $\text{sgn}(s - s') = 1$ almost everywhere.⁹ Then $z - |s - s'| = z - s + s'$ and we can, as before, invoke the linear-cancellation condition to see that $N_i = 0$.

If we select $Z_b = 3B$, $X_b = B$ and $Y_b = B$, then if $|z| > Z_b$, or $|x| > X_b$ or $|y| > Y_b$, then $|z| > Z_b$ or $|s| > B$ and thus we have proven the boundedness of the N_i domains.

J.2 Why the energy could be infinite if $s = x + y$

Previously, we pointed out that ϕ is a solution to Eq. (6) *almost everywhere*⁹ – but not everywhere. Instead, ϕ is a solution of Eq. (14), which differs from Eq. (6) by a term $S(x, y, z)$ originating from derivatives of the absolute values appearing in the definition of $s(x, y)$.

This naturally leads us to consider possible solutions ϕ that depend on $s(x, y) = x + y$. Because that definition of s doesn't involve absolute values, then the term S is absent.

Unfortunately, that definition of s does not lead to boundedness of the shift-vectors and, therefore, finiteness of the energy. We can easily see this by examining our proof of boundedness for the definition $s = |x| + |y|$. The proof demonstrates that when either $|z|$ or s is large, the shift vector is 0. However, boundedness is with respect to the coordinates x, y, z . When $s = |x| + |y|$, then s is large if either $|x|$ or $|y|$ are large. However, when $s = x + y$, we can have large x with $y \approx -x$ and therefore $s \approx 0$. Our boundedness-proof has nothing to say about situations where both s and z are small; therefore, in general, we can't show, for the case $s = x + y$ that the shift-vectors are 0 if either $|x|$ or $|y|$ are large.

For the rhomboidal-source ρ_{rh} , we now show that with $s = x + y$, the shift-vector would indeed have an unbounded domain and therefore, the energy would be infinite. Our source would now be

$$\rho_{\text{rh}}^{(s=x+y)}(s', z') = \rho_{\text{rhomb}}(x' + y', z'). \quad (159)$$

If we substitute that source in Eq. (29), then we find

$$N_x^{(s=x+y)} = \partial_x \phi = \frac{1}{4} \int_{-B}^B ds' \text{sgn}((x + y) - s') \rho_{\text{rh}}^{(s=x+y)}(s', z - |(x + y) - s'|). \quad (160)$$

Let $|x|$ be arbitrarily large, but $x = -y + 2$. Then

$$N_x^{(s=x+y)} = \partial_x \phi = \frac{1}{4} \int_{-B}^B ds' \text{sgn}(2 - s') \rho_{\text{rh}}^{(s=x+y)}(s', z - |2 - s'|). \quad (161)$$

$N_x^{(s=x+y)}(s, z)$ is obtained from Fig. (3), where x is substituted for s . When $x = -y + 2$ and $z = 0$, the coordinate $(s, z) = (2, 0)$. We see in Fig. (3) that $N_x(2, 0)$ is non-zero and thus, as claimed, the shift-vector component has an unbounded domain.

References

- [1] M. Alcubierre, “The warp drive: Hyper-fast travel within general relativity,” *Classical and Quantum Gravity*, vol. 11, no. 5, p. L73, May 1994. [Online]. Available: <https://dx.doi.org/10.1088/0264-9381/11/5/001>
- [2] C. Barceló, V. Boyanov, L. J. Garay, E. Martín-Martínez, and J. M. S. Velázquez, “Warp drive aerodynamics,” *Journal of High Energy Physics*, vol. 2022, no. 8, Aug 2022. [Online]. Available: <https://doi.org/10.1007%2Fjhep08%282022%29288>
- [3] G. Abellán, N. Bolívar, and I. Vasilev, “Alcubierre warp drive in spherical coordinates with some matter configurations,” *Eur. Phys. J. C*, vol. 83, no. 1, p. 7, 2023.
- [4] O. L. Santos-Pereira, E. M. C. Abreu, and M. B. Ribeiro, “Warp drive dynamic solutions considering different fluid sources,” in *16th Marcel Grossmann Meeting on Recent Developments in Theoretical and Experimental General Relativity, Astrophysics and Relativistic Field Theories*, 11 2021.
- [5] O. L. Santos-Pereira, E. M. C. Abreu, and M. B. Ribeiro, “Perfect fluid warp drive solutions with the cosmological constant,” *Eur. Phys. J. Plus*, vol. 136, no. 9, p. 902, 2021.
- [6] J. Natário, “Warp drive with zero expansion,” *Classical and Quantum Gravity*, vol. 19, no. 6, pp. 1157–1166, 2002. [Online]. Available: <https://doi.org/10.1088/0264-9381/19/6/308>
- [7] O. L. Santos-Pereira, “The warp drive: Superluminal travel within general relativity,” 2025. [Online]. Available: <https://arxiv.org/abs/2508.20348>
- [8] O. Santos-Pereira, E. Abreu, and M. Ribeiro, “Charged dust solutions for the warp drive spacetime,” *General Relativity and Gravitation*, vol. 53, 02 2021.
- [9] J. Fuchs, C. Helmerich, A. Bobrick, L. Sellers, B. Melcher, and G. Martire, “Constant velocity physical warp drive solution,” *Classical and Quantum Gravity*, vol. 41, no. 9, p. 095013, apr 2024. [Online]. Available: <https://doi.org/10.1088/1361-6382/ad26aa>

- [10] C. Helmerich, J. Fuchs, A. Bobrick, L. Sellers, B. Melcher, and G. Martire, “Analyzing warp drive spacetimes with warp factory,” *Classical and Quantum Gravity*, vol. 41, no. 9, p. 095009, apr 2024. [Online]. Available: <https://doi.org/10.1088/1361-6382/ad2e42>
- [11] G. Abellán, N. Bolívar, and I. Vasilev, “Spherical warp-based bubble with non-trivial lapse function and its consequences on matter content,” *Classical and Quantum Gravity*, vol. 41, no. 10, p. 105011, apr 2024. [Online]. Available: <https://doi.org/10.1088/1361-6382/ad3ed9>
- [12] N. Bolívar, G. Abellán, and I. Vasilev, “Warp bubble geometries with anisotropic fluids: A piecewise analytical approach,” *Annals of Physics*, vol. 481, no. 170147, July 2025. [Online]. Available: <https://doi.org/10.1016/j.aop.2025.170147>
- [13] C. Van Den Broeck, “On the (im)possibility of warp bubbles,” 1999. [Online]. Available: <https://arxiv.org/abs/gr-qc/9906050>
- [14] M. J. Pfenning and L. H. Ford, “The unphysical nature of warp drive,” *Classical and Quantum Gravity*, vol. 14, p. 1743, 1997. [Online]. Available: <https://arxiv.org/abs/gr-qc/9702026>
- [15] D. H. Coule, “No warp drive,” *Classical and Quantum Gravity*, vol. 15, pp. 2523–2527, 1998. [Online]. Available: <https://doi.org/10.1088/0264-9381/15/9/020>
- [16] P. F. González-Díaz, “On the warp drive space-time,” *Physical Review D*, vol. 62, p. 044005, 2000. [Online]. Available: <https://doi.org/10.1103/PhysRevD.62.044005>
- [17] H. G. White, “A discussion of space-time metric engineering,” *General Relativity and Gravitation*, vol. 35, no. 11, pp. 2025–2033, 2003. [Online]. Available: <https://doi.org/10.1023/A:1026247026218>
- [18] H. White, J. Vera, A. Han, A. R. Bruccoleri, and J. MacArthur, “Worldline numerics applied to custom casimir geometry generates unanticipated intersection with alcubierre warp metric,” *The European Physical Journal C*, vol. 81, no. 7, p. 677, 2021. [Online]. Available: <https://doi.org/10.1140/epjc/s10052-021-09484-z>
- [19] R. J. Low, “Speed limits in general relativity,” *Classical and Quantum Gravity*, vol. 16, no. 2, p. 543–549, Jan. 1999. [Online]. Available: <http://dx.doi.org/10.1088/0264-9381/16/2/016>

- [20] J. Santiago, S. Schuster, and M. Visser, “Generic warp drives violate the null energy condition,” *Physical Review D*, vol. 105, no. 6, mar 2022. [Online]. Available: <https://doi.org/10.1103/PhysRevD.105.064038>
- [21] B. Shoshany, “Lectures on faster-than-light travel and time travel,” 2019, <https://arxiv.org/pdf/1907.04178>.
- [22] S. W. Hawking, “Chronology protection conjecture,” *Physical Review D*, vol. 46, no. 2, p. 603, 1992. [Online]. Available: <https://doi.org/10.1103/PhysRevD.46.603>
- [23] K. D. Olum, “Superluminal travel requires negative energies,” *Physical Review Letters*, vol. 81, pp. 3567–3570, 1998. [Online]. Available: <https://doi.org/10.1103/PhysRevLett.81.3567>
- [24] A. E. Everett, “Warp drive and causality,” *Physical Review D*, vol. 53, pp. 7365–7368, 1996. [Online]. Available: <https://doi.org/10.1103/PhysRevD.53.7365>
- [25] M. Visser, “From wormhole to time machine: Comments on hawking’s chronology protection conjecture,” *Physical Review D*, vol. 47, pp. 554–565, 1993. [Online]. Available: <https://doi.org/10.1103/PhysRevD.47.554>
- [26] —, “Hawking’s chronology protection conjecture: Singularity structure of the quantum stress-energy tensor,” *Nuclear Physics B*, vol. 416, pp. 895–906, 1994. [Online]. Available: [https://doi.org/10.1016/0550-3213\(94\)90560-6](https://doi.org/10.1016/0550-3213(94)90560-6)
- [27] —, “The quantum physics of chronology protection,” in *The Future of Theoretical Physics and Cosmology: Celebrating Stephen Hawking’s 60th Birthday*, G. W. Gibbons, E. P. S. Shellard, and S. J. Drake, Eds. Cambridge University Press, 2003. [Online]. Available: <https://arxiv.org/abs/gr-qc/0204022>
- [28] J. L. Friedman and A. Higuchi, “Topological censorship and chronology protection,” *Annalen der Physik*, vol. 15, pp. 109–128, 2006. [Online]. Available: <https://doi.org/10.1002/andp.200510172>
- [29] S. Liberati, “Do not mess with time: Probing faster than light travel and chronology protection with superluminal warp drives,” in *The Handbook of Spacetime*, A. Ashtekar and V. Petkov, Eds. World Scientific, 2016, p. 120. [Online]. Available: https://doi.org/10.1142/9789813226609_0120

- [30] B. Shoshany and B. Snodgrass, “Warp Drives, Rest Frame Transitions, and Closed Timelike Curves,” 9 2023.
- [31] E. W. Lentz, “Breaking the warp barrier: Hyper-fast solitons in Einstein-Maxwell-plasma theory,” *Classical and Quantum Gravity*, vol. 38, no. 7, p. 075015, Mar 2021. [Online]. Available: <https://dx.doi.org/10.1088/1361-6382/abe692>
- [32] E. Lentz, “Hyper-fast positive energy warp drives,” in *16th Marcel Grossmann Meeting on Recent Developments in Theoretical and Experimental General Relativity, Astrophysics and Relativistic Field Theories*, 12 2021.
- [33] R. Arnowitt, S. Deser, and C. W. Misner, “Republication of: The dynamics of general relativity,” *General Relativity and Gravitation*, vol. 40, no. 9, pp. 1997–2027, aug 2008. [Online]. Available: <https://doi.org/10.1007%2Fs10714-008-0661-1>
- [34] E.ourgoulhon, “3+1 formalism and bases of numerical relativity,” 2007, <https://doi.org/10.48550/arXiv.gr-qc/0703035>.
- [35] S. D. B. Fell and L. Heisenberg, “Positive energy warp drive from hidden geometric structures,” *Class. Quant. Grav.*, vol. 38, no. 15, p. 155020, 2021.
- [36] M. Frasca, R. M. Liberati, and M. Rossi, “Warping effects in strongly perturbed metrics,” *MDPI Physics*, vol. 2, no. 4, pp. 665–678, 2020.
- [37] F. Carneiro, S. Ulhoa, J. Maluf, and J. da Rocha-Neto, “On the total energy conservation of the alcubierre spacetime,” *Journal of Cosmology and Astroparticle Physics*, vol. 2022, no. 07, p. 030, jul 2022. [Online]. Available: <https://doi.org/10.1088/1475-7516/2022/07/030>
- [38] G. Huey, “Membrane models as a means of propulsion in general relativity: super-luminal warp-drive that satisfies the weak energy condition,” *Classical and Quantum Gravity*, vol. 41, no. 13, p. 135007, jun 2024. [Online]. Available: <https://doi.org/10.1088/1361-6382/ad4e00>
- [39] K. Clough, T. Dietrich, and S. Khan, “What no one has seen before: gravitational waveforms from warp drive collapse,” *The Open Journal of Astrophysics*, vol. 7, Jul. 2024. [Online]. Available: <http://dx.doi.org/10.33232/001c.121868>

- [40] H. Pettit, “Faster than light travel is possible, scientist claims,” *New York Post*, Mar 2021. [Online]. Available: <https://nypost.com/2021/03/12/faster-than-light-travel-is-possible-scientist-claims/>
- [41] M. Borunda, “Warp drives: Physicists investigate faster-than-light space travel,” *Astronomy Magazine*, April 2021. [Online]. Available: <https://www.astronomy.com/space-exploration/warp-drives-physicists-investigate-faster-than-light-space-travel/>
- [42] R. Gast and Spektrum, “Star trek’s warp drive leads to new physics,” *Scientific American*. [Online]. Available: <https://www.scientificamerican.com/article/star-treks-warp-drive-leads-to-new-physics/>
- [43] B. Skuse, “Spacecraft in a ‘warp bubble’ could travel faster than light, claims physicist,” *Physics World*, Mar 2021. [Online]. Available: <https://physicsworld.com/a/spacecraft-in-a-warp-bubble-could-travel-faster-than-light-claims-physicist/>
- [44] F. Neukart, “Toward the stars: Technological, ethical, and sociopolitical dimensions of interstellar exploration,” *Space Policy*, vol. 72, p. 101676, 2025. [Online]. Available: <https://www.sciencedirect.com/science/article/pii/S0265964624000675>
- [45] J. Houran and H. Bauer, “‘Fringe Science’—A Tautology, Not Pariah,” *Journal of Scientific Exploration*, vol. 36, no. 2, pp. 207–217, 2022.
- [46] B. Koberlein, “Alcubierre gives us an update on his ideas about warp drives,” *Universe Today*, Mar 2021. [Online]. Available: <https://www.universetoday.com/articles/alcubierre-gives-us-an-update-on-his-ideas-about-warp-drives>
- [47] M. Wagh, “A groundbreaking scientific discovery just gave humanity the keys to interstellar travel,” *Popular Mechanics*, May 2024. [Online]. Available: <https://www.popularmechanics.com/science/a60941082/light-speed-warp-drive-breakthrough/>